[20] E. Koivunen, B. Wang, E. Ruoslahti, Phage libraries displaying cyclic peptides with different ring sizes: ligand specificities of the RGD-directed integrins, Biotechnology (NY) 13 (1995) 265–270.
[21] N. Maeda, Y. Takeuchi, M. Takada, Y. Sadzuka, Y. Namba, N. Oku, Anti-neovascular therapy by use of tumor neovasculature-targeted long-circulating liposome, J. Control. Release 100 (2004) 41–52.
[22] F. Pastorino, C. Brignole, D. Marimpietri, M. Cilli, C. Gambini, D. Ribatti, R. Longhi, T.M. Allen, A. Corti, M. Ponzoni, Vascular damage and anti-angiogenic effects of tumor vessel-targeted liposomal chemotherapy, Cancer Res. 63 (2003) 7400–7409.
[23] N. Oku, K. Doi, Y. Namba, S. Okada, Therapeutic effect of adriamycin encapsulated in long-circulating liposomes on Meth-A-sarcoma-bearing mice, Int. J. Cancer 58 (1994) 415–419.
[24] J.M. Saul, A.V. Annapragada, R.V. Bellamkonda, A dual-ligand approach for enhancing targeting selectivity of therapeutic nanocarriers, J. Control. Release 114 (2006) 277–287.
[25] K. Shimizu, T. Asai, C. Fuse, Y. Sadzuka, T. Sonobe, K. Ogino, T. Taki, T. Tanaka, N. Oku, Applicability of anti-neovascular therapy to drug-resistant tumor: Suppression of drug-resistant P388 tumor growth with neovessel-targeted liposomal adriamycin, Int. J. Pharm. 296 (2005) 133–141.

Journal of Controlled Release 141 (2010) 208–215

Contents lists available at ScienceDirect

Journal of Controlled Release

journal homepage: www.elsevier.com/locate/jconrel

Temperature-dependent transfer of amphotericin B from liposomal membrane of AmBisome to fungal cell membrane

Kosuke Shimizu [a], Masaaki Osada [a], Koji Takemoto [b], Yutaka Yamamoto [b], Tomohiro Asai [a], Naoto Oku [a,*]

[a] Department of Medical Biochemistry and Global COE program, School of Pharmaceutical Sciences, University of Shizuoka, 52-1 Yada, Suruga-ku, Shizuoka 422-8526, Japan
[b] Dainippon Sumitomo Pharma Co., Ltd., 1-98 Kasugade Naka 3-Chome, Konohana-ku, Osaka 554-0022, Japan

ARTICLE INFO

Article history:
Received 18 April 2009
Accepted 22 September 2009
Available online 6 October 2009

Keywords:
AmBisome
Temperature-dependency
Cell wall
Ergosterol
Membrane fluidity

ABSTRACT

Liposomal amphotericin B (AMPH-B), also known as AmBisome, exhibits a potent antifungal effect through its binding to ergosterol contained within the fungal cell membrane. However, the mechanism responsible for the movement of AmBisome-derived AMPH-B to the fungal cell membrane through the cell wall is not yet clear. Therefore, in the present study we aimed at elucidating this mechanism operating in *Saccharomyces cerevisiae*. AmBisome showed its antifungal effect against *S. cerevisiae* at 35 °C but not at 4 °C, whereas free AMPH-B was effective at both temperatures. A significant difference in the amount of AMPH-B transferred to the fungal cells between incubation at 4 and 35 °C was also observed when AmBisome was used. Confocal microscopic study, however, indicated that NBD-labeled AmBisome was localized on the surface of the fungal cells at either temperature. To decrease the affinity of AMPH-B for the liposomal membrane, we entrapped AMPH-B in fluid liposomes containing egg yolk phosphatidylcholine (EPC) instead of hydrogenated soy PC (HSPC). These liposomes showed the antifungal effect even at 4 °C. On the contrary, AMPH-B in liposomes containing ergosterol (Erg-AmB) instead of cholesterol showed a significantly weaker antifungal effect at 35 °C with reduced transfer of AMPH-B to the fungal cells. These results suggest that not the binding of AmBisome to target cells but the transfer of AMPH-B from liposomal membrane of AmBisome to the cell membrane is critical for the antifungal activity of AmBisome. This transfer is dependent on the temperature, fluidity of the liposomal membrane, and the affinity of AMPH-B for the fungal cell membrane.

© 2009 Elsevier B.V. All rights reserved.

1. Introduction

Since patients with infectious diseases caused by certain bacteria or fungi are at a high risk for death, the development of effective drugs for these diseases is of great importance. Mycosis is an infectious disease caused by fungal invasion, and it is divided into 3 classes based on the infection site. Among them, infection by fungi at deep internal organ such as lung and brain is the most serious and is known as deep mycosis. Amphotericin B (AMPH-B), a drug with strong antifungal activity, is effective against deep mycosis and also has a wide antibacterial spectrum [1,2]. As to its mechanism of action, AMPH-B is known to bind to ergosterol contained in the fungal cell membrane, which binding induces a permeability change in the membrane [3,4]. Since AMPH-B also has the ability to bind to cholesterol to some extent [5], it causes side effects such as nephrotoxicity [6]. In order to reduce the side effects of AMPH-B, a liposomal formulation of AMPH-B, known as AmBisome, has been developed. AmBisome is a small unilamellar vesicle containing AMPH-B that is stably retained in the hydrophobic part of the liposomal membrane by complexing with liposomal cholesterol. Since liposomalization of AMPH-B prolongs the circulation of AMPH-B in the bloodstream and decreases the transfer of AMPH-B to cell-membrane cholesterol, the use of AmBisome reduces the side effects of AMPH-B [7–11]. The mechanism of transfer of AMPH-B from AmBisome to the fungal membrane is still unclear, since AmBisome retains the drug in the liposomal membrane rather tightly. By electron microscopy Adler-Moore et al. previously examined the localization of liposomal lipids of AmBisome after exposure to fungal cells such as *Candida glabrata* and *Aspergillus fumigatus* and observed that AmBisome-derived lipids were distributed throughout the cytoplasm of the fungal cells after long-term incubation [12,13]. They also speculated that AmBisome has an affinity for the fungal cell wall and initially binds to it and that the liposomal lipids from AmBisome become dispersed throughout the cytoplasm after damage to the fungal cell membrane caused by AMPH-B released from disrupted AmBisome [13]. Their report indicates that the transfer of AmBisome-derived AMPH-B to the fungal cell membrane is a key step in the action of AmBisome against fungi.

In the present study, we aimed at elucidating the mechanism underlying the transfer of AMPH-B from AmBisome to the fungal cell membrane by using *Saccharomyces cerevisiae* as a model fungal cell. *S. cerevisiae* has a thick cell wall similar to that of other fungal cells [14].

Abbreviations: AMPH-B, amphotericin B; EPC, egg yolk phosphatidylcholine; EPG, egg yolk phosphatidylglycerol; DSPG, distearoylphosphatidylglycerol; HSPC, hydrogenated soy phosphatidylcholine; NBD-PE, *N*-4-nitrobenzo-2-oxa-13-diazol phosphatidylethanolamine.

* Corresponding author. Tel.: +81 54 264 5701; fax: +81 54 264 5705.
E-mail address: oku@u-shizuoka-ken.ac.jp (N. Oku).

0168-3659/$ – see front matter © 2009 Elsevier B.V. All rights reserved.
doi:10.1016/j.jconrel.2009.09.019

At first, we examined the temperature dependence of AmBisome activity against *S. cerevisiae*, and observed that, unlike AMPH-B, the antifungal activity of AmBisome was drastically suppressed at a low temperature. Then, we examined the localization of AmBisome in yeast cells at different temperatures by confocal laser-scanning microscopy and measured the amount of AMPH-B taken up into the cells. The transfer of AMPH-B from AmBisome to the cell and the antifungal activity of the liposomes were increased by raising the incubation temperature. Interestingly, AMPH-B in a fluid liposomal membrane was taken up into the cells more easily and was fungicidal at a low temperature. On the contrary, AMPH-B in ergosterol-containing liposomes was taken up into the cells in less amount; and the cytotoxic action was suppressed even at a high temperature. The results indicate the importance of translocation of AMPH-B from AmBisome to the cells in its antifungal activity.

2. Materials and methods

2.1. Reagents

AmBisome was the product of Dainippon Sumitomo Pharma Co., Ltd. (Osaka, Japan) Hydrogenated soy phosphatidylcholine (HSPC), distearoylphosphatidylglycerol (DSPG), egg yolk phosphatidylcholine (EPC), egg yolk phosphatidylglycerol (EPG), and cholesterol were gifts from Nippon Fine Chemical Co., Ltd. (Hyogo, Japan). Amphotericin B (AMPH-B), ergosterol, and *N*-4-nitrobenzo-2-oxa-13-diazol phosphatidylethanolamine (NBD-PE) were purchased from The United States Pharmacopeial Convention, Inc. (Rockville, MD, U.S.A.), Sigma-Aldrich Co. (St Louis, MO, U.S.A.), and Avanti Polar Lipids, Inc. (Alabaster, AL, U.S.A.), respectively. Rhodamine-dextran (10 kDa) was purchased from Wako Pure Chemical Industries, Ltd.

2.2. Yeast cell culture

Yeast cells of the *S. cerevisiae* ATCC 9763 (ATCC, U.S.A.) were used as a model of fungal cells in this experiment. They were colonized on YPD/agar medium and kept at 4 °C. Before experimental use, a single colony was picked up and grown in YPD medium with shaking at 30 °C for at least 12 h; and the OD_{600} of the cell suspension was adjusted to 0.1 using RPMI 1640 medium (Sigma-Aldrich Co.) buffered to pH 7.0 with 0.165 M MOPS (Dojindo Laboratories, Kumamoto, Japan).

2.3. Preparation of liposomes

AmBisome (liposomal AMPH-B) was composed of HSPC, DSPG, cholesterol, and AMPH-B (10:4:5:2 as a molar ratio). AmBisome solution was prepared by hydration of lyophilized AmBisomal components with ultrapure water. For preparation of NBD-labeled AmBisome, the lyophilized AmBisomal components were firstly dissolved in chloroform, after which NBD-PE solution was added to them. Then, they were lyophilized again with *t*-butanol and rehydrated with succinate-buffered solution (pH 5.5). Unincorporated NBD-PE was removed by gel filtration chromatography with a PD-10 column. For preparation of AmBisome encapsulating rhodamine-dextran, the lyophilized AmBisomal components were hydrated with rhodamine-dextran solution; and then free rhodamine-dextran was removed by column chromatography with Sepharose™ 4 Fast Flow (GE Healthcare UK Ltd., England). AMPH-B in liposomes containing ergosterol (Erg-AmB) was prepared with HSPC, DSPG, ergosterol, and AMPH-B (10:4:5:2 as a molar ratio). The thin lipid film containing AMPH-B was hydrated with succinate-buffered solution with 9% sucrose at 60 °C and freeze-thawed with liquid nitrogen for 3 cycles. The obtained liposomal solution was sized by sonication. Unincorporated AMPH-B was removed by column chromatography with Sepharose™ 4 Fast Flow. Liposomal AMPH-B composed of highly fluid phospholipids (Egg-AmB) was prepared with EPC, EPG, cholesterol, and AMPH-B (10:4:5:2 as a molar ratio) in the similar manner as used to prepare Erg-AmB. The particle size of each liposome was measured by dynamic light scattering analysis with a Zetasizer Nano (Malvern Instruments, Malvern, U.K.) and was about 100 nm in diameter.

2.4. Colony formation assay

Each liposomal AMPH-B diluted in succinate-buffered solution with 9% sucrose or free AMPH-B dissolved in 0.1% DMSO (final conc.) at a concentration of 20 μM as AMPH-B was added to a yeast cell suspension and incubated in MOPS-buffered RPMI 1640 medium at 4 or 35 °C for 0.5 or 3 h. Then, the cell suspension was centrifuged and washed twice with PBS. The cell pellet was resuspended in PBS and plated on YPD/agar medium. After 24 h of incubation at 30 °C, the number of colonies formed was counted.

2.5. Confocal microscopy

NBD-labeled liposomal AMPH-B (20 μM) was added to a yeast cell suspension, which was then incubated in MOPS-buffered RPMI 1640 medium at 4 or 35 °C for 3 or 24 h with shaking. After having been washed 3 times with PBS, the cells were fixed with 4% paraformaldehyde and stained with Fluorescent Brightener 28 (Sigma-Aldrich Co., U.S.A.) for cell-wall imaging. After another 3 washes with PBS, the cells were attached to MAS-coated glass slides (Matsunami Glass Ind., Ltd., Japan) by centrifugation, and then localization of liposomes in yeast cells was observed under an LSM510 META confocal laser-scanning microscope (Carl Zeiss, Inc., Germany).

2.6. Measurement of the amount of AMPH-B transferred to yeast cells

Liposomal AMPH-B (20 μM) was added to a yeast cell suspension, which was then incubated in MOPS-buffered RPMI 1640 medium with shaking at 4 or 35 °C for 0.5 or 3 h. After having been washed with PBS, the cells were disrupted by using glass beads with shaking and sonication, and AMPH-B in the cells was extracted with methanol. After centrifugation, the methanol extract was evaporated; and the residual AMPH-B was dissolved in the mobile phase for HPLC analysis. The HPLC conditions were the following: Column, TSKgel ODS-100Z 4.6×250 mm (Tosoh Co., Japan); mobile phase, acetonitrile and 2.5 mM EDTA (pH 5.0), 4:6 (v/v); temperature, 35 °C; injection volume, 50 μL; flow rate, 1.0 mL/min; and UV detection, 405 nm. Smart Chrom software was used for control of the HPLC system and data processing.

In the inhibition experiment, AmBisome was added to a yeast cell suspension, which was subsequently incubated in the presence or absence of drug free cholesterol liposomes (Cho-Lip) or vacant ergosterol liposomes (Erg-Lip) in MOPS-buffered RPMI 1640 medium. After a 3-h incubation, the amount of AMPH-B transferred to the cells was measured.

2.7. Investigation of AmBisome disruption

Rhodamine-encapsulating AmBisome was added to different numbers of yeast cells (OD_{600} = 0.1 or 0.3), and the cells were incubated in MOPS-buffered RPMI 1640 medium for 0.5 or 3 h at 4 or 35 °C. After centrifugation for washing, the supernatant medium was collected and ultracentrifuged to separate the intact AmBisome into the pellet. The resulting supernatant was then collected, and the fluorescence intensity of the rhodamine-dextran that had been released into the medium from AmBisome was measured.

2.8. FRAP experiment

NBD-labeled AmBisome and Egg-AmB were similarly prepared as described above and then gradually frozen to make giant-sized liposomes. Then, these liposomes were applied on MAS-coated slide glasses and dried in the dark at room temperature for overnight. FRAP experiments were performed with LSM510 META confocal laser-

scanning microscope according to the protocol of LSM510 for FRAP experiment.

2.9. Statistic analysis

The variance in a group was evaluated by use of the *F*-test, and the differences among the groups were evaluated by using Student's *t*-test.

3. Results

3.1. Temperature-dependent antifungal activity of AmBisome against S. cerevisiae

To confirm the temperature dependence of AmBisome antifungal activity, we evaluated the effect of AmBisome against *S. cerevisiae* at 4 or 35 °C by using the colony formation assay. As shown Fig. 1A, AmBisome showed time-dependent antifungal activity against yeast cells at 35 °C. Free AMPH-B showed stronger antifungal activity than AmBisome, and no colonies were found even after just 0.5 h of incubation with it at 35 °C. On the other hand, the antifungal effect of AmBisome was significantly reduced at 4 °C incubation (Fig. 1B), and the number of colonies was quite similar to that of the control, suggesting the antifungal effect of AmBisome to be temperature-dependent. In contrast, free AMPH-B showed strong fungicidal activity even at this temperature. These results are summarized in Fig. 1C.

3.2. Binding of AmBisome to the surface of yeast cells

In general, intact liposome is unable to pass through the fungal cell wall due to its particle size. However, the cell wall penetration of AmBisome has not been fully elucidated, and it is not clear when or where AmBisome-derived AMPH-B is transferred to the fungal cell membrane. To elucidate the mechanism, we prepared NBD-labeled AmBisome and used confocal laser-scanning microscopy to observe its localization in yeast cells after exposure. AmBisome was observed to bind to the surface of yeast cells after a 3-h exposure at 35 °C (Fig. 2A). Especially, AmBisome often bound to budding or interface site of yeast cells. Furthermore, AmBisome-derived fluorescence was observed in the cytoplasm after 24 h of incubation at this temperature (Fig. 2B). Although liposomes without encapsulated AMPH-B also bound to the cell surface, they were not incorporated into the cytoplasm after a 24-h incubation (data not shown). On the other hand, similar to the 35 °C incubation, AmBisome bound to the cell surface after a 3-h incubation at 4 °C (Fig. 2A). However, unlike that at 35 °C, AmBisome-derived fluorescence was present only on the cell surface after 24 h of incubation at the lower temperature (Fig. 2B). The cellular uptake of AmBisome after 24 h incubation at 35 °C, would be the result of permeability increase in cell membrane caused by AMPH-B transferred to the membrane, since the distribution of NBD-labeled AmBisome in *S. cerevisiae* in the presence of free AMPH-B at 4 °C, NBD-labeled AmBisome was observed in the cytosol (data not shown).

3.3. Temperature-dependent transfer of AMPH-B from AmBisome to yeast cells

Next, we compared the amount of AMPH-B transferred to yeast cells at different incubation temperatures. AmBisome was added to the yeast cell suspension, and the cells were incubated at 4 or 35 °C. Thereafter, the amount of AMPH-B transferred to the cells was determined by HPLC. As a result, the amount of AMPH-B in the yeast cells was reduced at 4 °C of incubation (Fig. 3), suggesting that this transfer mechanism of AMPH-B from AmBisome is temperature-dependent.

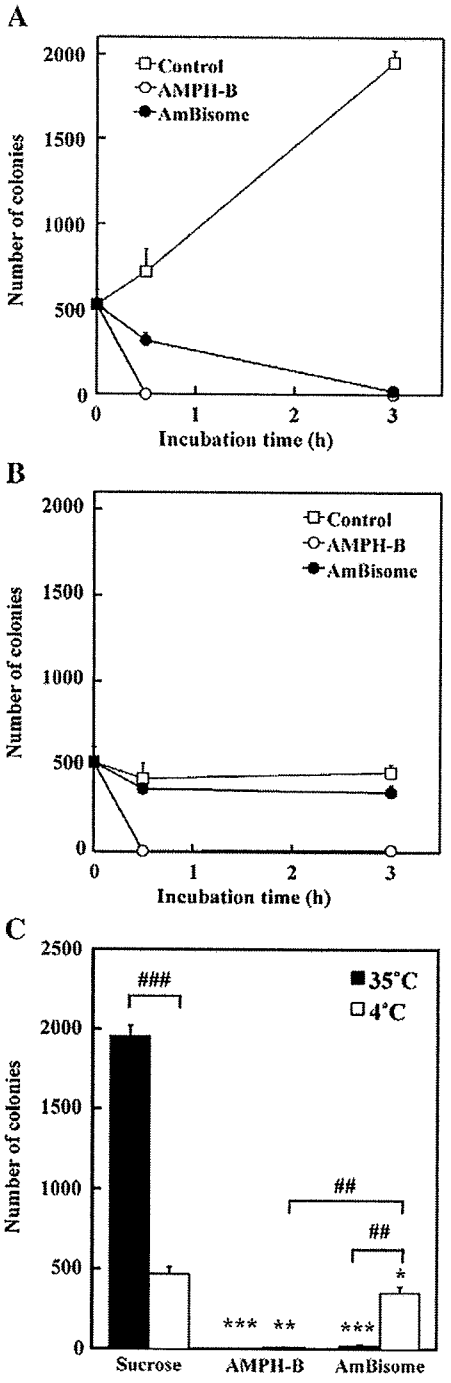

Fig. 1. Temperature-dependent antifungal activity of AmBisome against *Saccharomyces cerevisiae*. After the optical density of a *S. cerevisiae* suspension was adjusted to 0.1, sucrose, AMPH-B, or AmBisome (20 μM as AMPH-B) was added to the yeast cell suspension; and incubation was carried out at 35 °C (A) or 4 °C (B) for 0.5 or 3 h in MOPS-buffered RPMI 1640 medium. After the cells had been washed with PBS, they were plated on YPD/agar medium. After 24 h of incubation at 30 °C, the number of colonies formed was counted. The difference in activity between temperatures is also summarized (C). Significant differences are shown (* $P<0.05$, ** $P<0.01$, *** $P<0.001$ *vs.* Sucrose; ## $P<0.01$, ### $P<0.001$ as indicated by the brackets).

3.4. Disruption of AmBisome at the yeast cell surface

It is not clear whether or not the disruption of AmBisome is a prerequisite for AMPH-B release from the liposomal membrane after

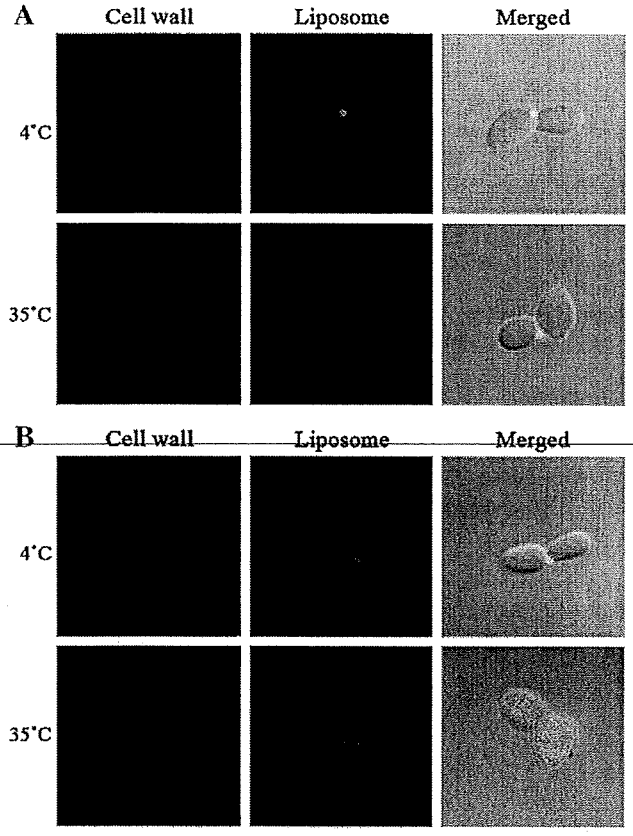

Fig. 2. Binding of AmBisome to cell wall of yeast cells. NBD-labeled AmBisome was added to yeast cell suspensions that were then incubated in MOPS-buffered RPMI 1640 medium at 4 or 35 °C for 3 h (A) or 24 h (B). Then, the yeast cell wall was stained with Fluorescent Brightener 28, and localization of AmBisome was observed with a confocal laser-scanning microscope. Green and blue images show AmBisome and the cell wall, respectively. Bar indicates 10 μm.

binding of AmBisome to the surface of yeast cells. To clarify this point, we prepared rhodamine-encapsulated AmBisome and investigated the disruption of the liposomes after exposure of the yeast cells to it.

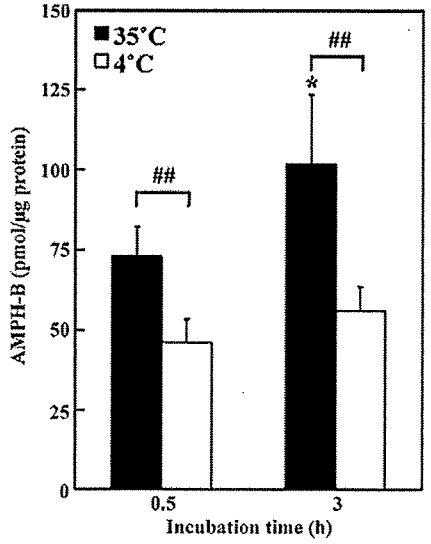

Fig. 3. Temperature-dependent transfer of AMPH-B to yeast cells. AmBisome was added to cell suspensions of *Saccharomyces cerevisiae* that were then incubated in MOPS-buffered RPMI 1640 medium at 4 or 35 °C for 0.5 or 3 h. After the cells had been washed with PBS, the amount of AMPH-B in the yeast cells was measured by HPLC. Significant differences are indicated (* $P<0.05$ *vs.* 35 °C; ## $P<0.01$, as indicated by the brackets).

When rhodamine-encapsulated AmBisome was incubated with yeast cells at a low density or number at 35 °C, the fluorescence of rhodamine released from AmBisome was very little, and most of the fluorescence was detected in the liposome fraction (Fig. 4A). A similar result was obtained even when the number of yeast cells was increased. Furthermore, there was no apparent difference in liposomal disruption between at 4 and 35 °C incubation (Fig. 4B). These results suggest that AmBisome was not disrupted at least until 3 h after binding to the cell surface and that AmBisome-derived AMPH-B was transferred to the fungal cell membrane without liposomal disruption.

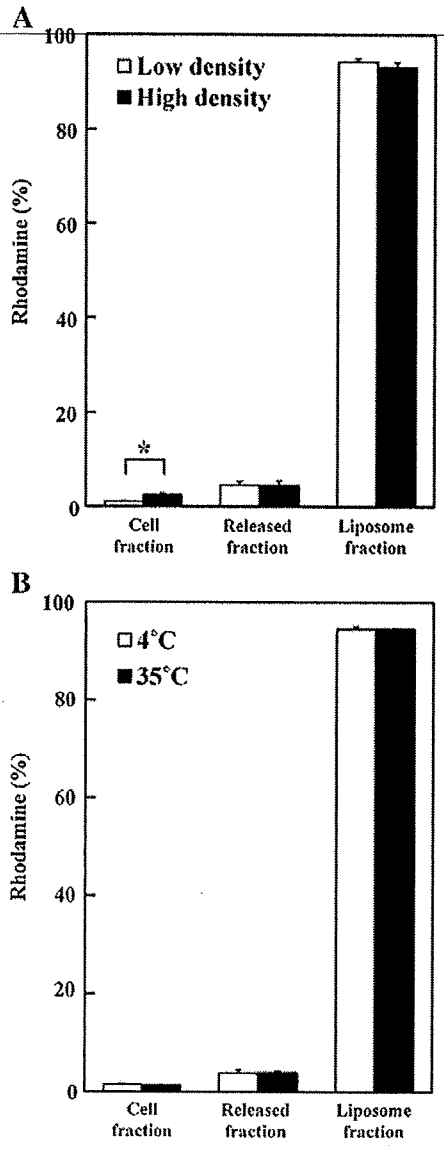

Fig. 4. Investigation of liposomal disruption during exposure of yeast cells to AmBisome. Rhodamine-encapsulating AmBisome was added to a suspension of *Saccharomyces cerevisiae* that had been adjusted to a low ($OD_{600}=0.1$) or high ($OD_{600}=0.3$) density, and the cells were then incubated in MOPS-buffered RPMI 1640 medium at 35 °C for 3 h (A). The culture medium was collected and ultracentrifuged to remove intact AmBisome. The fluorescence intensity of the rhodamine that had been released from rhodamine-encapsulating AmBisome into the medium was measured in the supernatant. Disruption of AmBisome at 4 °C was also examined (B). Asterisk shows a significant difference between bracketed values (* $P<0.05$).

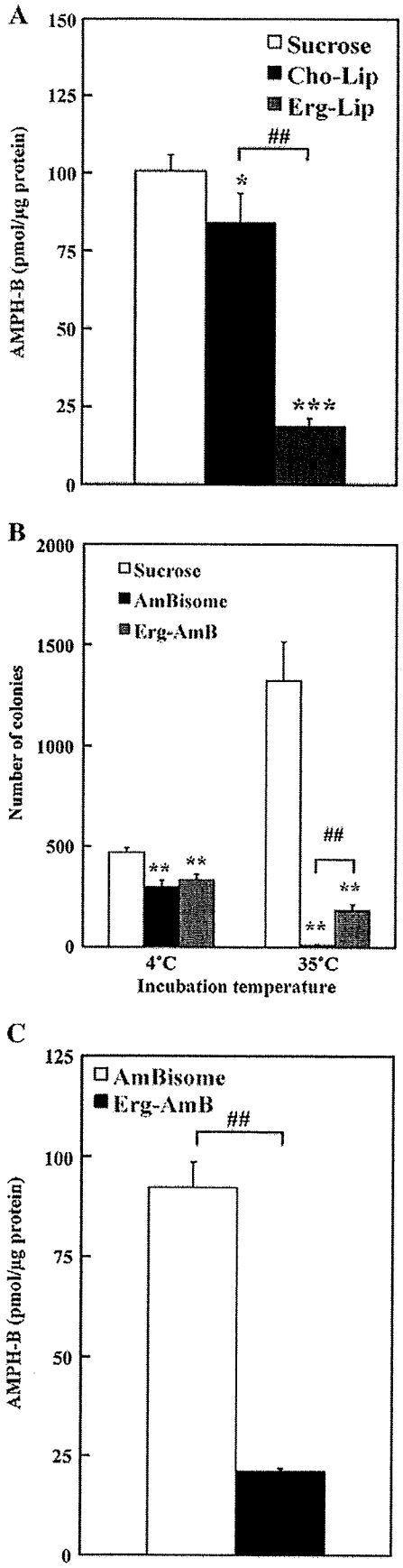

3.5. Importance of differential AMPH-B affinity for AmBisome and yeast cell membrane

To examine the importance of AMPH-B affinity for the fungal cell membrane during the transfer of AmBisome-derived AMPH-B to the membrane, we examined the transfer of AMPH-B to yeast cells in the presence of cholesterol liposomes (Cho-Lip) or ergosterol liposomes (Erg-Lip) in which AMPH-B was not entrapped. As a result, the transfer of AMPH-B from AmBisome was significantly reduced in the presence of Erg-Lip, whereas little inhibition was observed in the presence of Cho-Lip (Fig. 5A), confirming that the affinity of AMPH-B for ergosterol-containing membrane is stronger than that for cholesterol-containing one.

Next, we prepared liposomal AMPH-B containing ergosterol (Erg-AmB) instead of cholesterol and examined the antifungal activity of Erg-AmB against yeast cells. At 4 °C, the antifungal activity of Erg-AmB was attenuated just as in the case of AmBisome (Fig. 5B). However, at 35 °C Erg-AmB failed to kill all of the yeast cells whereas AmBisome completely destroyed them at this temperature (Fig. 5B). Furthermore, when the transfer of AMPH-B from Erg-AmB to the cells was investigated, the amount of AMPH-B in the cells was reduced after 3 h of incubation (Fig. 5C). These results indicate that ergosterol in the liposomes controlled the antifungal effect of liposomal AMPH-B and that the different affinity of AMPH-B for cholesterol and ergosterol played an important role in the transfer of AMPH-B to the fungal cell membrane.

3.6. Importance of liposomal membrane fluidity in temperature-dependent antifungal activity of AmBisome

Since the transfer of AMPH-B from AmBisome to the fungal cell membrane was dependent on the incubation temperature, we hypothesized that liposome membrane fluidity was a key factor in the transfer of AMPH-B. To examine the importance of membrane fluidity on the transfer of AMPH-B from AmBisome, we prepared AMPH-B liposomes composed of the highly fluid phospholipids EPC and EPG (Egg-AmB) instead of HSPC and DPPG. To measure the membrane fluidity of both liposomes, fluorescence recovery after photobleaching (FRAP) experiment was performed. NBD-labeled both liposomes were prepared, and FRAP measurement was recorded by using confocal laser scanning microscope (LSM510META). As a result, the fluorescence of NBD-PE in NBD-labeled Egg-AmB was recovered to more than 80% at 50 s after photobleaching and the diffusion coefficient was $8.2\times10^{-2}\mu m^2/s$, whereas the recovery of fluorescence in NBD-labeled AmBisome was little observed. This result indicates that liposome membrane fluidity of Egg-AmB is far higher than that of AmBisome. Then, the antifungal effect of Egg-AmB against *S. cerevisiae* was investigated at 4 or 35 °C incubation. Egg-AmB not only completely damaged yeast cells at 35 °C, but also showed the antifungal effect at 4 °C to some extent (Fig. 6A). When localization of NBD-labeled Egg-AmB in the yeast cells was observed under the confocal laser-scanning microscope, the fluorescence of Egg-AmB was present in the cytoplasm at both 4 and 35 °C after a 3-h incubation (Fig. 6B), whereas similar images were observed only after a 24-h incubation with AmBisome at 35 °C (Fig. 2B). Furthermore, the increase in the amount

Fig. 5. Effect of ergosterol on antifungal activity of AmBisome. AmBisome was added to yeast cell suspensions of *Saccharomyces cerevisiae* that were then incubated in the absence or presence of drug-free cholesterol liposome (Cho-Lip) or drug-free ergosterol liposome (Erg-Lip) for 3 h at 35 °C in MOPS-buffered RPMI 1640 medium. Then, the amount of AMPH-B in the cells was measured (A). Yeast cells were also incubated with sucrose, AmBisome or liposomal AMPH-B containing ergosterol (Erg-AmB) at 4 or 35 °C for 3 h. After the cells had been washed with PBS, they were plated on YPD/agar medium. After a 24-h incubation at 30 °C, the number of formed colonies was counted (B). The amount of AMPH-B in yeast cells after 3 h of incubation at 35 °C was also measured (C). Significant differences are shown (* $P<0.05$, ** $P<0.01$, *** $P<0.001$ *vs.* Sucrose; ## $P<0.01$, as indicated by the bracket).

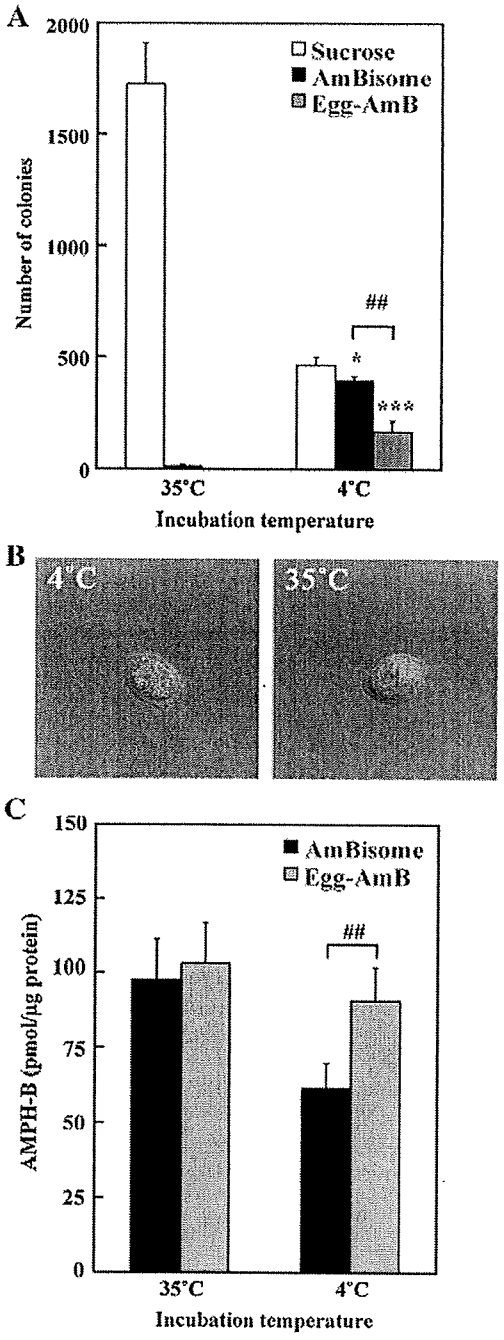

Fig. 6. Effect of liposome-membrane fluidity on antifungal activity of AmBisome. Cell suspensions of *Saccharomyces cerevisiae* were incubated with sucrose, AmBisome or liposomal AMPH-B composed of EPC and EPG (Egg-AmB) at 4 or 35 °C for 3 h in MOPS-buffered RPMI 1640 medium. After the cells had been washed with PBS, they were plated on YPD/agar medium. After 24 h of incubation at 30 °C, the number of colonies formed was counted (A). Localization of NBD-labeled Egg-AmB after a 3-h incubation at 4 or 35 °C was observed (B) and the amount of AMPH-B in the yeast cells after 3 h of incubation at 4 or 35 °C was also measured (C). Significant differences are shown (* $P<0.05$, *** $P<0.001$ vs. Sucrose; ## $P<0.01$, as indicated by the bracket).

of AMPH-B transferred from Egg-AmB to the cells after the 4 °C incubation was obvious (Fig. 6C). These results suggest that liposomal membrane fluidity was involved in the transfer of AMPH-B from AmBisome to the fungal cell membrane and indicate that AMPH-B in fluid liposomes would be easier to transfer to other membranes with high affinity for AMPH-B.

4. Discussion

It is known that liposomalization or polymerization of a drug often enables enhancement of the therapeutic effects and reduces the side effects by improving the pharmacokinetics and pharmacodynamics of the original drug in the body [15,16]. The liposomal antifungal drug AmBisome is a representative example of a liposome that incorporates AMPH-B in its membrane, enhances the stability of AMPH-B in the bloodstream and reduces the side effects of the drug [9,10]. AmBisome shows a potent antifungal effect against fungal cells such as *Candida albicans*, *Cryptococcus neoformans*, and *Aspergillus fumigatus*, resulting in the successful treatment of deep mycosis caused by them [17,18]. AmBisome exerts its effect by the binding of AMPH-B from AmBisome to ergosterol in the fungal cell membrane, which binding enhances the permeability of the fungal cell membrane and promotes the leakage of cellular substances and subsequent fungal cell death [3,19]. Thus, the transfer of AMPH-B from AmBisome to the fungal cell membrane is a key step for AmBisome to manifest its antifungal activity. In the case of other liposomal drugs, the release of the encapsulated drug from the liposome is critical for drug activity. For example, liposomal doxorubicin shows a potent cytotoxic effect against various kinds of cancer. The action mechanism of liposomal doxorubicin is considered to be as follows: Liposomal doxorubicin is incorporated into the cells by the endocytic pathway, the liposome is disrupted in lysosomes, and the encapsulated doxorubicin is released and transferred to nuclei to damage the cell. On the other hand, it is expected that the action mechanism of AmBisome against fungal cells would be different from that of other liposomal drugs against mammalian cells, since fungal cells possess a protective cell wall around their cell membrane, unlike mammalian cells [20]. In fact, it has not been fully clarified whether AmBisome can pass through the cell wall or not. In the present study, we aimed at elucidating the action mechanism of AmBisome, especially the mechanism of the transfer of AMPH-B from the liposome to ergosterol in the fungal cell membrane.

We firstly focused on the temperature dependence of AmBisome activity by comparing the antifungal effect of AmBisome against *S. cerevisiae* at 4 and 35 °C. As a result, AmBisome showed strong time-dependent antifungal activity at 35 °C, whereas free AMPH-B eradicated the yeast cells completely after just a 0.5-h incubation (Fig. 1A), indicating that AmBisome required a certain period of time to show its antifungal activity compared with AMPH-B. Furthermore, AmBisome did not show the activity at 4 °C, whereas AMPH-B showed strong activity at this same temperature (Fig. 1B, C). These results suggest that antifungal activity of AmBisome is dependent on the release and transfer of its AMPH-B to the fungal cell membrane. This temperature-dependent AmBisome activity would not be due to a difference in the localization of AmBisome in yeast cells, since AmBisome bound to yeast cells similarly at both 4 and 35 °C (Fig. 2A). Similar binding of AmBisome at 4 and 35 °C was also observed after a 0.5-h incubation (data not shown). These data also support the idea that the release and transfer of AMPH-B from AmBisome is critical for the antifungal efficacy instead of a temperature-dependent amount of AmBisome binding. In fact, the amount of AMPH-B transferred from AmBisome increased in a temperature-dependent manner (Fig. 3).

Adler-Moore et al. previously reported that gold-labeled AmBisome binds to the fungal cell wall, as observed by electron microscopy [13]. In our study, AmBisome actually bound to the cell wall and was topically observed to become localized at the budding or interface site of *S. cerevisiae* after a 3-h incubation at either 4 or 35 °C (Fig. 2A). In their review article Lesage et al. stated that the structure and components of the yeast cell wall change according to cell growth and are especially different during bud emergence and at the mother/daughter interface [21]. Thus, we hypothesize that these regions of the cell wall are susceptible to binding by AmBisome and that its

AMPH-B is transferred to the fungal cell membrane at these regions in a temperature-dependent manner. However, further research will be needed to elucidate whether AmBisome directly interacts with the fungal cell membrane or not.

Furthermore, AmBisome-derived fluorescence was present in the cytoplasm after 24 h of incubation at 35 °C but not at 4 °C (Fig. 2B). We speculate that the fungal cell death causes the entry of AmBisome into the cytoplasm.

We next examined the possible disruption of AmBisome for the transfer of AMPH-B to the fungal cell membrane. As a result, AmBisome-derived rhodamine release was minimal after exposure to the drug, even when the number of yeast cells was increased or the incubation temperature was changed (Fig. 4). These results indicate that the transfer of AMPH-B from AmBisome occurred at least until 3 h after attachment to the outside of fungal cells without disruption of the liposomal architecture of AmBisome.

Finally, to identify the key factor for the transfer of AMPH-B from AmBisome, we prepared liposomal AMPH-B with different lipid compositions and investigated the effect of lipid composition on AmBisome-induced antifungal activity. When AMPH-B was incorporated into liposomes containing ergosterol instead of cholesterol, the antifungal effect against *S. cerevisiae* was significantly reduced compared with that of AmBisome at 35 °C, where the membrane fluidity is considered to be similar (Fig. 5B). In addition, the amount of transferred AMPH-B to the yeast cells from Erg-AmB was decreased (Fig. 5C). It is known that the affinity of AMPH-B for ergosterol is about 10 times higher than that for cholesterol [22]. Thus, this result suggests that liposomal ergosterol prevented the release of AMPH-B from liposomes, the consequence being suppression of the transfer of AMPH-B from AmBisome to the fungal cell surface. A number of studies have been presented about the reason for the high affinity of AMPH-B to ergosterol in comparison with that to choresterol. Recently, Baran et al. suggested that AmB-ergosterol-AmB aggregates simulated of 2:1 stoichiometry retain significantly higher stability and relatively rigid, "sandwich" geometry due to Van der Waals forces and the intermolecular hydrogen bonds [23]. In contrast, cholesterol does not form this sandwich geometry that would be the reason for the low affinity of AMPH-B to cholesterol in comparison with this to ergosterol [23].

On the contrary, when AMPH-B was incorporated into liposomes composed of high-fluidity phospholipids, namely, EPC and EPG, the antifungal effect against *S. cerevisiae* was observed even at 4 °C, where the membrane fluidity is rather low and AmBisome showed little effect (Fig. 6A). In addition, the amount of AMPH-B transferred to the yeast cells from Egg-AmB was increased (Fig. 6C). When localization of NBD-labeled Egg-AmB in the yeast cells was examined, the fluorescence of Egg-AmB was present in the cytoplasm even after 0.5 h of incubation (Fig. 6B). It is known that the phase-transition temperature of EPC and HSPC is about −10 °C and 55 °C, respectively. When the membrane fluidity of Egg-AmB and AmBisome was compared using NBD-PE by FRAP experiment, the membrane fluidity of Egg-AmB is higher than that of AmBisome. According to the result, it is reasonable that the transfer of AMPH-B from Egg-AmB to the fungal cell membrane would occur at the low temperature. Thus, these results suggest that the increased membrane fluidity enhanced the release of AMPH-B from AmBisome and stability of AMPH-B in the liposomal membrane is the key factor for the biological activity of liposomal AMPH-B.

According to the report by Legrand et al., the critical micelle concentration (CMC) of AMPH-B was 0.1 μM in aqueous solution. They showed that the concentration of free AMPH-B released by AmBisome at 1 μg/ml (1.08 μM) was about 0.08 μg/ml (0.09 μM), which was below the CMC of AMPH-B [24]. We investigated the release of AMPH-B from AmBisome at high concentration (2.22 mM) in MOPS-buffered RPMI 1640 medium at room temperature using an ultrafiltration method. As a result, time-dependent release of AMPH-B was not observed (0.293 and 0.369 μM at 0 and 24 h after incubation, respectively; 0.013% and 0.017% of total AMPH-B in AmBisome), suggesting that AmBisome is quite stable, but allows the release of a little amount of AMPH-B (data not shown). Based on such information and results obtained in the present study, we hypothesized that ergosterol in the fungal cell membrane may be able to increase the amount of AMPH-B released from AmBisome or induce the continuous release of AMPH-B from AmBisome without direct interaction to AmBisome after AmBisome attachment to the fungal cell wall.

5. Conclusion

Our present study demonstrated that AmBisome bound to the cell wall of yeast cells and that the AMPH-B from AmBisome was transferred to the yeast cell membrane without obvious disruption of the liposome formulation. Furthermore, we demonstrated that the transfer of AMPH-B was dependent on temperature and fluidity of the liposome membrane.

Acknowledgements

The authors thank all members of the Department of Medical Biochemistry at the University of Shizuoka for their helpful advice in this study.

Appendix A. Supplementary data

Supplementary data associated with this article can be found, in the online version, at doi:10.1016/j.jconrel.2009.09.019.

References

[1] M.E. Klepser, E.J. Wolfe, R.N. Jones, C.H. Nightingale, M.A. Pfaller, Antifungal pharmacodynamic characteristics of fluconazole and amphotericin B tested against *Candida albicans*, Antimicrob. Agents Chemother. 41 (6) (1997) 1392–1395.
[2] L. Ostrosky-Zeichner, K.A. Marr, J.H. Rex, S.H. Cohen, Amphotericin B: time for a new "gold standard", Clin. Infect. Dis. 37 (3) (2003) 415–425.
[3] B.E. Cohen, Concentration- and time-dependence of amphotericin-B induced permeability changes across ergosterol-containing liposomes, Biochim. Biophys. Acta 857 (1) (1986) 117–122.
[4] I. Fournier, J. Barwicz, P. Tancrede, The structuring effects of amphotericin B on pure and ergosterol- or cholesterol-containing dipalmitoylphosphatidylcholine bilayers: a differential scanning calorimetry study, Biochim. Biophys. Acta 1373 (1) (1998) 76–86.
[5] K.M. Wasan, G. Lopez-Berestein, The interaction of liposomal amphotericin B and serum lipoproteins within the biological milieu, J. Drug Target 2 (5) (1994) 373–380.
[6] R. Sabra, R.A. Branch, Amphotericin B nephrotoxicity, Drug Saf 5 (2) (1990) 94–108.
[7] I. Bekersky, R.M. Fielding, D.E. Dressler, J.W. Lee, D.N. Buell, T.J. Walsh, Plasma protein binding of amphotericin B and pharmacokinetics of bound versus unbound amphotericin B after administration of intravenous liposomal amphotericin B (AmBisome) and amphotericin B deoxycholate, Antimicrob. Agents Chemother. 46 (3) (2002) 834–840.
[8] J. Adler-Moore, R.T. Proffitt, Effect of tissue penetration on AmBisome efficacy, Curr. Opin. Investig. Drugs 4 (2) (2003) 179–185.
[9] K. Takemoto, Y. Yamamoto, Y. Ueda, Evaluation of antifungal pharmacodynamic characteristics of AmBisome against *Candida albicans*, Microbiol. Immunol. 50 (8) (2006) 579–586.
[10] K. Takemoto, Y. Yamamoto, Y. Ueda, Y. Sumita, K. Yoshida, Y. Niki, Comparative study on the efficacy of AmBisome and Fungizone in a mouse model of pulmonary aspergillosis, J. Antimicrob. Chemother. 57 (4) (2006) 724–731.
[11] E. Briones, C.I. Colino, J.M. Lanao, Delivery systems to increase the selectivity of antibiotics in phagocytic cells, J. Control Release 125 (3) (2008) 210–227.
[12] J. Adler-Moore, AmBisome targeting to fungal infections, Bone Marrow Transplant. 14 (Suppl 5) (1994) S3–7.
[13] J. Adler-Moore, R.T. Proffitt, AmBisome: liposomal formulation, structure, mechanism of action and pre-clinical experience, J. Antimicrob. Chemother 49 (Suppl 1) (2002) 21–30.
[14] V.J. Cid, A. Duran, F. del Rey, M.P. Snyder, C. Nombela, M. Sanchez, Molecular basis of cell integrity and morphogenesis in *Saccharomyces cerevisiae*, Microbiol. Rev. 59 (3) (1995) 345–386.
[15] T.M. Allen, P.R. Cullis, Drug delivery systems: entering the mainstream, Science 303 (5665) (2004) 1818–1822.
[16] G. Gaucher, M.H. Dufresne, V.P. Sant, N. Kang, D. Maysinger, J.C. Leroux, Block copolymer micelles: preparation, characterization and application in drug delivery, J. Control Release 109 (1–3) (2005) 169–188.

[17] J.P. Adler-Moore, S.M. Chiang, A. Satorius, D. Guerra, B. McAndrews, E.J. McManus, R.T. Proffitt, Treatment of murine candidosis and cryptococcosis with a unilamellar liposomal amphotericin B formulation (AmBisome), J. Antimicrob. Chemother 28 (Suppl B) (1991) 63–71.
[18] A.C. Leenders, P. Reiss, P. Portegies, K. Clezy, W.C. Hop, J. Hoy, J.C. Borleffs, T. Allworth, R.H. Kauffmann, P. Jones, F.P. Kroon, H.A. Verbrugh, S. de Marie, Liposomal amphotericin B (AmBisome) compared with amphotericin B both followed by oral fluconazole in the treatment of AIDS-associated cryptococcal meningitis, AIDS 11 (12) (1997) 1463–1471.
[19] M. Baginski, H. Resat, E. Borowski, Comparative molecular dynamics simulations of amphotericin B-cholesterol/ergosterol membrane channels, Biochim. Biophys. Acta 1567 (1–2) (2002) 63–78.
[20] M. Kirkham, R.G. Parton, Clathrin-independent endocytosis: new insights into caveolae and non-caveolar lipid raft carriers, Biochim. Biophys. Acta 1745 (3) (2005) 273–286.
[21] G. Lesage, H. Bussey, Cell wall assembly in *Saccharomyces cerevisiae*, Microbiol. Mol. Biol. Rev. 70 (2) (2006) 317–343.
[22] J.D. Readio, R. Bittman, Equilibrium binding of amphotericin B and its methyl ester and borate complex to sterols, Biochim. Biophys. Acta 685 (2) (1982) 219–224.
[23] M. Baran, E. Borowski, J. Mazerski, Molecular modeling of amphotericin B-ergosterol primary complex in water II, Biophys. Chem. 141 (2–3) (2009) 162–168.
[24] P. Legrand, M. Cheron, L. Leroy, J. Bolard, Release of amphotericin B from delivery systems and its action against fungal and mammalian cells, J. Drug Target 4 (5) (1997) 311–319.

Preventive Effect of Green Tea Catechins on Experimental Tumor Metastasis in Senescence-Accelerated Mice

Kosuke SHIMIZU,[a] Naomi KINOUCHI SHIMIZU,[a] Wakako HAKAMATA,[a] Keiko UNNO,[b] Tomohiro ASAI,[a] and Naoto OKU*,[a]

[a] *Department of Medical Biochemistry and Global COE Program, University of Shizuoka; and* [b] *Laboratory of Bioorganic Chemistry, School of Pharmaceutical Sciences, University of Shizuoka; 52–1 Yada, Suruga-ku, Shizuoka, Shizuoka 422–8526, Japan.* Received August 27, 2009; accepted October 5, 2009; published online October 29, 2009

Successful avoidance of the immune surveillance system is critical for the development of a blood–borne metastasis. Previous findings suggest that experimental tumor metastasis was enhanced in senescence-accelerated mice prone 10 (SAMP10) due to a reduction in immune surveillance potential with age. In the present study, water containing green tea (GT)-catechins was freely given to SAMP10 mice, and the chemopreventive effect of GT-catechin intake on tumor metastasis was examined. Natural killer cell activity, which is an indicator of immune surveillance potential and is reduced in control mice with age, was maintained by GT-catechin intake. The early accumulation of lung-metastatic K1735M2 melanoma cells in lungs after intravenous injection of the cells and subsequent experimental lung metastasis was investigated in mice given GT-catechins. The accumulation at 6 and 24 h after injection of K1735M2 cells was significantly suppressed, and the number of lung-metastatic colonies was significantly reduced, in comparison with those in control mice. The results suggest that GT-catechin intake prevented the experimental tumor metastasis in aged SAMP10 mice *via* its inhibition of a reduction in immune surveillance potential with age.

Key words aging; tumor metastasis; green tea catechin; immune surveillance

Tumor metastasis is a key step in the development of a tumor and becomes a critical trigger for the death of a patient. Hematogenous metastasis is established by a series of steps, which begin with the dissociation from primary sites and culminate with the formation of metastatic colonization.[1] This process is greatly dependent on surrounding host factors such as host resistance to cancerous cells.[2,3] In a previous study, we demonstrated that the early accumulation of metastatic tumor cells in a target organ after intravenous injection of the cells and following tumor metastasis were enhanced by reduction of the host immune surveillance potential,[4,5] suggesting that avoidance of the surveillance associated with immune cells, such as natural killer (NK) cells, was a critical step for the completion of an experimental tumor metastasis.

The senescence-accelerated mice prone (SAMP) strain has been established as a mouse model for aging research[6] and exhibits a more accelerated senescence process than normal mice.[7,8] By using this model, we found that the immune surveillance potential of 8-month-old aged SAMP10 mice was lower than that of 2-month-old young mice, and that the experimental lung metastasis was significantly induced in aged mice. These data suggest that the aging process produces an environment susceptible to metastatic tumor cells in the bloodstream to complete metastasis, and that such an environment is produced with age due to the reduced immune surveillance potential.[9]

Green tea (GT)-catechins are functional polyphenols, and are known to have various actions, such as antibiotic, anti-inflammatory, antioxidative, and anti-cancer effects. It is anticipated they will become useful as a functional food that promotes human health and longevity. Although animal studies have shown that GT-catechin treatment suppressed tumorigenesis, tumor growth, and tumor angiogenesis,[10,11] the crucial mechanism of the action of GT-catechin against cancer has not been fully elucidated. Our previous study demonstrated that (−)-epigallocatechin gallate (EGCG, a major component of GT-catechins) suppressed tumor angiogenesis through the inhibition of membrane type-1 matrix metalloproteinase (MT-1MMP) activity and subsequent induction of dormancy of solid tumor growth.[12,13] Tachibana *et al.* also reported that 67-kDa laminin receptors are a receptor for EGCG and that EGCG treatment inhibited the receptor-mediated signaling pathway and subsequent tumor cell growth.[14,15] Several reports have described various such approaches to treat and prevent cancer using GT-catechins. In the present study, we hypothesized that GT-catechin intake modulates the immune surveillance potential in aged mice, and enhances the susceptibility to experimental tumor metastasis. To prove this, we exposed SAMP10 mice to GT-catechin in their drinking water for an extended period of time (aged/catechin mice) and examined their NK activity as an indicator of immune surveillance potential. We then also examined the accumulation of K1735M2 melanoma cells in the lungs, the target organ, after intravenous injection of the cells as well as the preventive effect of GT-catechin intake on experimental tumor metastasis.

MATERIALS AND METHODS

Animals SAMP10 mice were purchased from Japan SLC Inc. (Shizuoka, Japan). They began to show several senescence symptoms such as brain atrophy and dehairing from about 6 months-old. Since their immune surveillance potential was adequately reduced at 8 months-old,[9] we used 8-month-old or older SAMP10 mice as an appropriate model for the cancer prone age (aged SAMP10 mice). In another group of aged mice (aged/catechin SAMP10 mice), water containing 0.02% (w/v) GT-catechins (Polyphenon70S, Mitsui Norin Co., Ltd., Tokyo) was given *ad libitum* beginning

* To whom correspondence should be addressed. e-mail: oku@u-shizuoka-ken.ac.jp

© 2010 Pharmaceutical Society of Japan

at the age of 1-month-old. Polyphenon70S is a crude extract from green tea and contains various kinds of catechins such as (−)-epigallocatechin gallate (EGCG), which is the main component, and (−)-epicatechin gallate (ECG), (−)-epigallocatechin (EGC), and epicatechin (EC). The contents of the various catechins in Polyphenon70S are shown in Table 1 (Information was provided by Mitsui Norin Co., Ltd.). Animal care and experiments were performed in accordance with the Guidelines for the Care and Use of Laboratory Animals of the University of Shizuoka.

Cells Highly lung-metastatic, murine K1735M2 melanoma cells were kindly provided by Dr. Jun Yokota of the National Cancer Center (Tokyo, Japan). These cells were cultured in Dulbecco's modified Eagle's medium (DMEM) containing 10% fetal bovine serum (FBS, Japan Bio Serum Co., Ltd., Hiroshima, Japan) at 37 °C in the presence of 5% CO_2 in a humid atmosphere. NK-sensitive YAC-1 cells were purchased from the RIKEN Bioresource Center Cell Bank (Ibaraki, Japan) and cultured in RPMI1640 medium containing 10% FBS at 37 °C in the presence of 5% CO_2.

Experimental Lung Metastatic Model K1735M2 cells (5×10^4 cells/mouse) were intravenously injected into 2-month-old, 8-month-old, or 13-month-old SAMP10 mice *via* a tail vein and metastatic colonies were allowed to form in their lungs. In the chemoprevention experiment, K1735M2 cells were injected into 8-month-old aged or 8-month-old aged/catechin SAMP10 mice. Twenty-one days after injection of the tumor cells, the animals were sacrificed under diethylether anesthesia, and their perfused lungs were isolated. Tumor metastasis was evaluated by counting the number of metastatic colonies on the surface of the lungs.

NK Activity Assay To measure the NK activity, spleen cells were used as effector cells. Spleen of aged or aged/catechin SAMP10 mice was harvested, and the splenocytes were carefully flushed several times with an 18 G needle-tipped syringe and passed through nylon mesh to prepare the single cell suspension. The resultant cells were washed twice after removal of erythrocytes, and the number of cells was adjusted to 1.25, 2.5, and 5×10^6 cells/ml. On the other hand, to prepare target cells for ^{51}Cr release assay, mouse NK-sensitive lymphoma YAC-1 cells were used. The cells were incubated with $Na_2{}^{51}CrO_4$ solution (GE Healthcare U.K., Ltd., England) for 60 min at 37 °C for ^{51}Cr-radiolabeling. After removal of free ^{51}Cr, the number of radiolabeled cells was adjusted to 1×10^5 cells/ml. NK activity of aged or aged/catechin SAMP10 mice was measured by ^{51}Cr release assay as follows: Both the effector and the target cells were mixed in 96-well-plates and the plates were incubated for 4 h at 37 °C. After centrifugation of the cell suspension, radioactivity in the supernatant was measured with a gamma counter. Spontaneous release and maximum release were determined by adding RPMI medium containing 10% FBS or 0.1% TritonX-100 solution to the target cell suspension. Specific cytotoxicity of NK cells was determined using the following formula:

$$\%\ \text{lysis} = \frac{(\text{experimental release} - \text{spontaneous release})}{(\text{maximum release} - \text{spontaneous release})} \times 100$$

Distribution of Metastatic Tumor Cells K1735M2 cells were radiolabeled with 5-[^{125}I]iodo-2′-deoxyuridine ([^{125}I]IUdR, GE Healthcare U.K., Ltd.) as described previously.[16] Briefly, these cells were incubated overnight with [^{125}I]IUdR at 37 °C in the presence of 5% CO_2. After incubation, the cells were collected and centrifuged to remove unincorporated [^{125}I]IUdR, and the number of cells was adjusted to 1×10^4 cells/mouse for injection. These cells were intravenously injected into 8-month-old aged and 8-month-old aged/catechin SAMP10 mice. At 6 and 24 h after the injection, the mice were sacrificed under anesthesia with diethylether to collect blood and organ (heart, lung, liver, spleen, and kidney) samples. The amount of accumulation of tumor cells in each organ was determined by radioactivity. Distribution data are presented as % injected dose per tissue. The total weight of blood was assumed to be 7.56% of the body weight.

Table 1. Composition of Green Tea Catechins

GT-catechins	Content (w/w, %)
Epigallocatechin (EGC)	16.5
Epicatechin (EC)	5.7
Epigallocatechin gallate (EGCG)	34.5
Epicatechin gallate (ECG)	10.1
Gallocatechin gallate (GCG)	2.9
Catechin gallate (CG)	0.6

Information of the content was provided from Mitsui Norin Co., Ltd.

Statistic Analysis The variance in a group was evaluated using the *F*-test, and the differences among each group were evaluated using Student's *t*-test.

RESULTS

Enhanced Experimental Tumor Metastasis with Age in SAMP10 Mice We first investigated whether this enhancement of tumor metastasis is dependent on the degree of aging or not. Therefore, 2-month-old, 8-month-old, and 13-month-old SAMP10 mice were prepared and an experimental tumor metastasis assay was performed using K1735M2 melanoma cells. As in a previous report, the number of metastatic colonies in the lungs of 8-month-old aged mice was larger than that in 2-month-old young mice. In 13-month-old aged SAMP10 mice, the number of colonies was further increased (Fig. 1). This result suggested that the susceptibility to experimental tumor metastasis in SAMP10 mice increased in an age-dependent manner.

Effect of GT-Catechin Intake on NK Activity in Aged SAMP10 Mice We assumed that GT-catechin intake could suppress the reduction of immune surveillance potential with aging. Two groups of SAMP10 mice were grown in the same environment except that aged/catechin SAMP10 mice were given water containing 0.02% Polyphenon70S instead of normal water beginning at 1-month-old. When these mice reached 8 months-old, their NK activity was examined. The results of ^{51}Cr release assay showed that NK activity in aged/catechin SAMP10 mice was significantly higher than that of aged SAMP10 mice for every effector cells/target cells (E/T) ratio (Fig. 2), suggesting that GT-catechin intake suppressed the attenuation of immune surveillance potential with age.

Suppression of Tumor Cell Accumulation in Lung by GT-Catechin Intake We next confirmed the early accumulation of lung-metastatic K1735M2 cells after intravenous in-

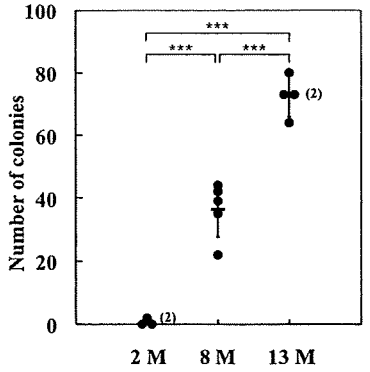

Fig. 1. Age-Dependent Increase in Experimental Tumor Metastasis in SAMP10 Mice

K1735M2 cells (5×10^4 cells/mouse) were intravenously injected into 2-month-old (n=4), 8-month-old (n=5), and 13-month-old SAMP10 mice (n=4), and the number of metastatic colonies in the lungs was counted on day 21 after the tumor cell implantation. The circles in the graph show the number of colonies in individual mice and black bars show the average number of colonies in each mouse. Asterisks indicate the significant differences (***p<0.001). Similar results were obtained in a separate experiment.

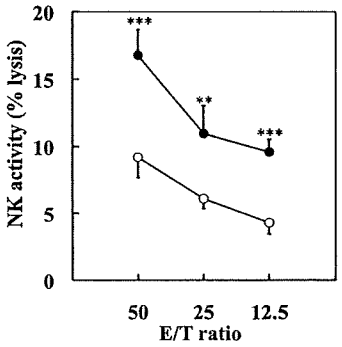

Fig. 2. Recovery of NK Activity by GT-Catechin Intake in Aged SAMP10 Mice

Cytotoxicity of NK cells from the spleen (E: effector cells) of aged (○) and aged/catechin (●) SAMP10 mice against ^{51}Cr-labeled YAC-1 target cells (T: target cells) was examined as described in Materials and Methods. The radioactivity detected in supernatant medium was measured by a gamma counter, and the NK activity was determined. Significant differences from aged control mice are indicated (**p< 0.01; ***p<0.001). Similar results were obtained in a separate experiment.

jection in aged and aged/catechin SAMP10 mice, since GT-catechin intake suppressed the reduction in immune surveillance potential with age. As shown in Fig. 3A, the accumulation of [^{125}I]IUdR-labeled K1735M2 cells in the lungs of aged/catechin mice was lower than that in aged SAMP10 mice at 6 h after the intravenous injection of the cells. Furthermore, this difference in the accumulation was maintained up to 24 h (Fig. 3B). These results supported the idea that GT-catechin intake suppresses the attenuation of immune surveillance potential, and therefore the clearance of metastatic tumor cells from the target organ is not impaired.

Preventive Effect of GT-Catechin Intake on Experimental Lung Metastasis in Aged SAMP10 Mice To investigate the preventive effect of GT-catechin intake on experimental tumor metastasis in old age, lung-metastatic K1735M2 tumor cells (5×10^5 cells/mouse) were injected into the bloodstream of 8-month-old aged, or aged/catechin SAMP10 mice, and then the number of lung-metastatic colonies was determined on day 21 after injection. The number of metastatic colonies in the lung of aged/catechin SAMP10 mice was far less than that in aged SAMP10 mice given normal water (Fig. 4).

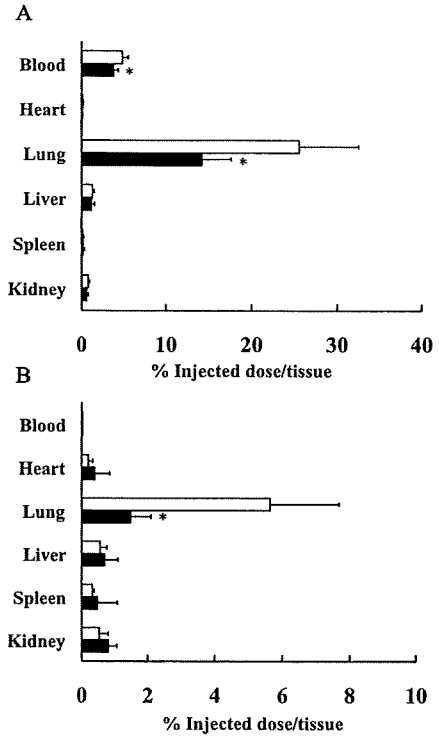

Fig. 3. Distribution of [^{125}I]IUdR-Labeled K1735M2 Melanoma Cells in SAMP10

[^{125}I]IUdR-labeled K1735M2 melanoma cells (1×10^4 cells/mouse) were injected into aged (open column) and aged/catechin (closed column) SAMP10 mice. The columns indicate the percent accumulation of [^{125}I]IUdR-labeled K1735M2 melanoma cells 6 (A) and 24 (B) h after injection. Significant differences from aged mice are indicated (*p<0.05). Distribution experiments were performed in two more separate experiments, and similar results were obtained.

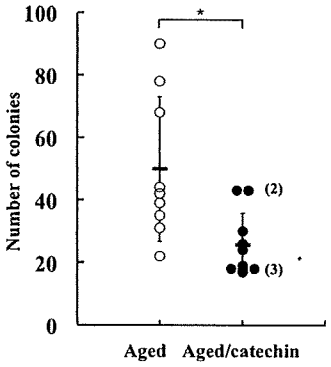

Fig. 4. Preventive Effect of GT-Catechin Intake of Experimental Tumor Metastasis in Aged SAMP10 Mice

K1735M2 cells (5×10^4 cells/mouse) were intravenously injected into aged (n=9) and aged/catechin SAMP10 mice (n=10) and the metastatic colonies in the lungs were counted on day 21 after tumor implantation. The circles in the graph show the number of colonies in individual mice and black bars show the average number of colonies in each mouse. Asterisks indicate significant differences (*p<0.05). Similar results were obtained in a separate experiment.

DISCUSSION

Senescence is accompanied by various changes in the body, and the internal environment in aged people is different from that in young people. Young people are able to maintain

body homeostasis, and their capacity to defend against foreign substances such as exogenous antigens is superior to that of aged people. Although the mechanism of aging is quite complicated, the accumulation of reactive oxygen species (ROS) in the body is considered to be an important factor in aging.[17] While the relationship between ROS production and cancer development has already been demonstrated, cancer usually starts to develop in middle age or later, suggesting that the aging process is involved in cancer development.[18,19] Our previous study demonstrated that the aging process caused the enhancement of susceptibility to experimental tumor metastasis in senescence-accelerated mice and the reason why it occurs was suggested to be due to a reduction in immune surveillance potential against metastatic tumor cells with age.[9] These findings suggest that the maintenance of a healthy internal environment in aged animals would improve the age-related weakening of the protective effect against experimental metastasis.

To maintain body homeostasis in a favorable condition, a number of functional components have been developed, of which GT-catechin is a well-known example.[20] Many researchers have studied GT-catechin functions and the multifunctional effects of GT-catechins against cancer have been demonstrated.[11] Young animals have been widely used in these basic studies on cancer prevention since it takes a long time to prepare aged animals. It is uncertain, however, whether this situation reflects aged humans, who have high cancer rates, and if these functional components are truly effective at preventing cancer. In the present study, we used SAMP mice as a model to investigate the preventive effect of GT-catechin intake against tumor metastasis in old age.

We first prepared SAMP10 mice of different ages and examined the difference in blood–borne metastasis after intravenous injection of K1735 melanoma cells with age. As shown in Fig. 1, the number of metastatic colonies increased with age. This result confirmed those of our previous study and demonstrated that tumor metastasis was accelerated in an age-dependent manner.[9] In an attempt to inhibit tumor metastasis in old age, we exposed aged SAMP10 mice to GT-catechin water (0.02% Polyphenon70S) for an extended period of time. When the daily intake volume of GT-catechin water was measured, the volume was about 10 ml/d/mouse and was almost the same as for the group given normal water.

At first, the cytotoxicity of splenocytes derived from aged and aged/catechin mice against NK-sensitive YAC-1 cells was measured as an indicator of immune surveillance potential, since the spleen possesses a lot of immune-related cells such as NK cells and plays a critical role in the systemic immune system. GT-catechin intake enhanced the NK activity of aged SAMP10 mice (Fig. 2). Since aging is thought to involve the accumulation of oxidative stress,[21,22] it is possible that an age-dependent burden of oxidative stress causes degradation of the immune defense system against the tumor cells. In actual fact, the cytotoxicity of NK cells is known to be dependent on oxidative stress and the activity is often reduced by ROS.[23] Ferrández *et al.* previously demonstrated that an age-dependent reduction in NK activity was improved by the existence of antioxidant agents such as ascorbic acid and α-tocopherol.[24] This result suggests that the antioxidant agents up-regulated NK activity through their protection against ROS. On the other hand, GT-catechins, especially EGCG, are known to work as potent radical scavengers and show antioxidative effects against various types of oxidative stress.[22,25] Unno *et al.* demonstrated that long-term intake of EGCG water up-regulated the level of antioxidative activity in the serum of aged SAMP10 mice.[26] Thus, we speculated that GT-catechin intake provided protection from the accumulation of oxidative stress and improved the reduced NK activity with age. We also reported that consumption of GT-catechin prevented the decline of glutathione peroxidase activity and provided protection from oxidative damage of protein in mouse brain of aged SAMP10.[27] This result also supports our present speculation that GT-catechin intake up-regulates the age-induced reduction in NK activity and has the effect in aged animals.

We next evaluated the effect of GT-catechin intake on blood–borne metastasis induced by intravenous injection of tumor cells. We previously demonstrated that defense against metastatic tumor cells by the immune surveillance system was observed in the early stage of tumor metastasis by use of positron emission tomography (PET).[4,5] In the study, we examined the relationship among the real-time trafficking of lung-metastatic B16BL6 cells, metastatic potential, and the number of the cells injected. When 1×10^4 cells were injected, the accumulation of the cells in the lung was less than one-tenth of that obtained with a 1×10^5 cell-injection. Metastasis was observed when 1×10^5 cells were injected, but not when 1×10^4 cells were injected. To clarify the roles of the immune defense system at the initial phase of metastasis, mice were treated with 2-chloroadenosine prior to the tumor cell challenge. As a result, this treatment suppressed not only metastasis but also the early accumulation of the cells in lungs. These results suggest that the immune surveillance, whose action was obvious at the low dose of challenged tumor cells, functions strongly at the initial phase but not at the advanced stages of the metastatic process.[5] Therefore, in the present study, we examined the biodistribution of [^{125}I]-labeled K1735M2 cells after intravenous injection and found that early accumulation of tumor cells in their metastatic site was reduced in aged/catechin SAMP10 mice, and this status was also observed at 24 h after injection (Fig. 3).

NK cells are one type of immune cell related to innate immunity, especially immune surveillance, and together with macrophages form the first lines of defense against exogenous agents and tumor cells. Therefore, this result suggested that suppressing the decrease in NK activity with age by GT-catechin intake suppressed the age-induced accumulation of tumor cells in the target organ at the early stage. Experimental tumor metastasis in aged SAMP10 mice was also suppressed by GT-catechin intake (Fig. 4). Shimizu *et al.* reported that daily intake of green tea extract protected against metachronous colorectal adenomas after surgical removal of primary tumors in a pilot study in humans.[28] Our results in the present study may partly explain their finding.

In conclusion, the results of the present study indicate that GT-catechin intake improved the reduction in immune surveillance potential, such as NK activity with age, and suppressed the age-related increase in the susceptibility to experimental tumor metastasis in SAMP10 mice. Thus, daily intake of green tea may provide protection against the weakening of immune surveillance activity with age and thus con-

tribute to human health and longevity. In the present study, SAMP mice were used as an aging model because the internal environment of the body of aged animals and their responses to chemopreventive agents are different from those of young animals. The usage of aged animals to investigate the therapeutic and preventive efficacy of chemopreventive agents may produce more predictable results for actual human cancers.

Acknowledgments The authors thank Dr. Jun Yokota of the National Cancer Center for donating the K1735M2 melanoma cells and Dr. Yukihiko Hara of Mitsui Norin Co., Ltd. for providing the Polyphenon70S. The authors also wish to thank all members of the Department of Medical Biochemistry at the University of Shizuoka for supporting the experiments and their helpful advice. This work was supported in part by the Global COE Program of the Ministry of Education, Culture, Sports, Science and Technology, MEXT, Japan.

REFERENCES

1) Mundy G. R., *Nat. Rev. Cancer*, **2**, 584—593 (2002).
2) Anisimov V. N., *Crit. Rev. Oncol. Hematol.*, **45**, 277—304 (2003).
3) Krtolica A., Campisi J., *Int. J. Biochem. Cell Biol.*, **34**, 1401—1414 (2002).
4) Kikkawa H., Tsukada H., Oku N., *Cancer*, **89**, 1626—1633 (2000).
5) Kikkawa H., Imafuku H., Tsukada H., Oku N., *FEBS Lett.*, **467**, 211—216 (2000).
6) Takeda T., Hosokawa M., Higuchi K., *Exp. Gerontol.*, **32**, 105—109 (1997).
7) Higuchi K., *Exp. Gerontol.*, **32**, 129—138 (1997).
8) Miyamoto M., *Exp. Gerontol.*, **32**, 139—148 (1997).
9) Shimizu K., Kinouchi Shimizu N., Asai T., Tsukada H., Oku N., *Biol. Pharm. Bull.*, **31**, 847—851 (2008).
10) Surh Y. J., *Nat. Rev. Cancer*, **3**, 768—780 (2003).
11) Khan N., Afaq F., Saleem M., Ahmad N., Mukhtar H., *Cancer Res.*, **66**, 2500—2505 (2006).
12) Oku N., Matsukawa M., Yamakawa S., Asai T., Yahara S., Hashimoto F., Akizawa T., *Biol. Pharm. Bull.*, **26**, 1235—1238 (2003).
13) Yamakawa S., Asai T., Uchida T., Matsukawa M., Akizawa T., Oku N., *Cancer Lett.*, **210**, 47—55 (2004).
14) Tachibana H., Koga K., Fujimura Y., Yamada K., *Nat. Struct. Mol. Biol.*, **11**, 380—381 (2004).
15) Umeda D., Yano S., Yamada K., Tachibana H., *J. Biol. Chem.*, **283**, 3050—3058 (2007).
16) Koike C., Watanabe M., Oku N., Tsukada H., Irimura T., Okada S., *Cancer Res.*, **57**, 3612—3619 (1997).
17) Benz C. C., Yau C., *Nat. Rev. Cancer*, **8**, 875—879 (2008).
18) Burns E. A., Leventhal E. A., *Cancer Control*, **7**, 513—522 (2000).
19) Campisi J., *Nat. Rev. Cancer*, **3**, 339—349 (2003).
20) Crespy V., Williamson G., *J. Nutr.*, **134**, 3431S—3440S (2004).
21) Mori A., Utsumi K., Liu J., Hosokawa M., *Ann. N.Y. Acad. Sci.*, **854**, 239—250 (1998).
22) Tobi S. E., Gilbert M., Paul N., McMillan T. J., *Int. J. Cancer*, **102**, 439—444 (2002).
23) Nakamura K., Matsunaga K., *Cancer Biother. Radiopharm.*, **13**, 275—290 (1998).
24) Ferrández M. D., Correa R., Del Rio M., De la Fuente M., *Exp. Gerontol.*, **34**, 675—685 (1999).
25) Frei B., Higdon J. V., *J. Nutr.*, **133**, 3275S—3284S (2003).
26) Unno K., Takabayashi F., Yoshida H., Choba D., Fukutomi R., Kikunaga N., Kishido T., Oku N., Hoshino M., *Biogerontology*, **8**, 89—95 (2007).
27) Unno K., Takabayashi F., Kishido T., Oku N., *Exp. Gerontol.*, **39**, 1027—1034 (2004).
28) Shimizu M., Fukutomi Y., Ninomiya M., Nagura K., Kato T., Araki H., Suganuma M., Fujiki H., Moriwaki H., *Cancer Epidemiol. Biomarkers Prev.*, **17**, 3020—3025 (2008).

Available online at www.sciencedirect.com

ScienceDirect

Nuclear Medicine and Biology 36 (2009) 295–303

NUCLEAR MEDICINE — AND — BIOLOGY

www.elsevier.com/locate/nucmedbio

Evaluation of *O*-[^{18}F]fluoromethyl-D-tyrosine as a radiotracer for tumor imaging with positron emission tomography☆

Takeo Urakami[a], Koichi Sakai[b], Tomohiro Asai[a], Dai Fukumoto[b], Hideo Tsukada[b], Naoto Oku[a,*]

[a]*Department of Medical Biochemistry and Global COE, University of Shizuoka Graduate School of Pharmaceutical Sciences, Yada, Suruga-ku, Shizuoka 422-8526, Japan*

[b]*PET Center, Central Research Laboratory, Hamamatsu Photonics K.K., Hamamatsu, Shizuoka 434-8601, Japan*

Received 14 April 2008; received in revised form 3 December 2008; accepted 24 December 2008

Abstract

O-[^{18}F]Fluoromethyl-D-tyrosine (D-[^{18}F]FMT) has been reported as a potential tumor-detecting agent for positron emission tomography (PET). However, the reason why D-[^{18}F]FMT is better than L-[^{18}F]FMT is unclear. To clarify this point, we examined the mechanism of their transport and their suitability for tumor detection. The stereo-selective uptake and release of enantiomerically pure D- and L-[^{18}F]FMT by rat C6 glioma cells and human cervix adenocarcinoma HeLa cells were examined. The results of a competitive inhibition study using various amino acids and a selective inhibitor for transport system L suggested that D-[^{18}F]FMT, as well as L-[^{18}F]FMT, was transported via system L, the large neutral amino acid transporter, possibly via LAT1. The in vivo distribution of both [^{18}F]FMT and [^{18}F]FDG in tumor-bearing mice and rats was imaged with a high-resolution small-animal PET system. In vivo PET imaging of D-[^{18}F]FMT in mouse xenograft and rat allograft tumor models showed high contrast with a low background, especially in the abdominal and brain region. The results of our in vitro and in vivo studies indicate that L-[^{18}F]FMT and D-[^{18}F]FMT are specifically taken up by tumor cells via system L. D-[^{18}F]FMT, however, provides a better tumor-to-background contrast with a tumor/background (contralateral region) ratio of 2.741 vs. 1.878 with the L-isomer, whose difference appears to be caused by a difference in the influence of extracellular amino acids on the uptake and excretion of these two isomers in various organs. Therefore, D-[^{18}F]FMT would be a more powerful tool as a tumor-detecting agent for PET, especially for the imaging of a brain cancer and an abdominal cancer.

© 2009 Published by Elsevier Inc.

Keywords: *O*-[^{18}F]Fluoromethyl tyrosine; D-isomer; Positron emission tomography (PET); System L transporter; Tumor imaging

1. Introduction

[^{18}F]FDG is the most widely used tracer for tumor detection with PET imaging. However, several limitations with [^{18}F]FDG have been reported, such as a high uptake in normal brain and heart and in inflammatory tissues [1]. In contrast, the accumulation of positron emitter-labeled amino acids was assumed to reflect enhanced amino acid transport, metabolism and protein synthesis. Therefore, these amino acid tracers have been used for detecting tumors especially those in the brain.

Positron emitter-labeled amino acids and their derivatives, such as 1-[^{11}C]methionine [2], methyl-[^{11}C]methionine [2,3], 1-[^{11}C]tyrosine [4], 1-[^{11}C]leucine [5], 1-[^{11}C]phenylalanine [6], 4-[^{18}F]fluoro-phenylalanine [7] and 2-[^{18}F]fluoro-L-tyrosine [8], have been proposed as PET imaging agents. Among these positron emitter-labeled amino acids, [^{11}C]methionine is widely used for tumor imaging with PET. Recently, several amino acid analogs, namely, *O*-[^{11}C]methyl-L-tyrosine [9], *O*-[^{18}F]fluoromethyl-L-tyrosine (L-[^{18}F]FMT) [9], *O*-[^{18}F]fluoroethyl-L-tyrosine [10,11], *O*-[^{18}F]fluoropropyl-L-tyrosine [12,13], [^{11}C]ethyonine [14] and [^{11}C]propionine [14], were synthesized and evaluated as PET imaging agents. These amino acid

☆ This study was supported by a grant from the Central Shizuoka Cooperation of Innovative Technology and Advanced Research in Evolution Area (City Area) supported by the Ministry of Education, Culture, Sports, Science and Technology of Japan (MEXT); and also by the Research and Development of Technology for Measuring Vital Function Merged with Optical Technology, MEXT; and by the Research and Development Project Aimed at Economic Revitalization, MEXT.

* Corresponding author. Tel.: +81 54 264 5701; fax: +81 54 264 5705.
E-mail address: oku@u-shizuoka-ken.ac.jp (N. Oku).

0969-8051/$ – see front matter © 2009 Published by Elsevier Inc.
doi:10.1016/j.nucmedbio.2008.12.012

analogues showed relatively low accumulation in normal peripheral tissue (low tissue-to-blood ratio), rapid blood clearance and a rather high amount of label remaining in tumor tissues (high tumor-to-blood ratio).

In contrast to L-isomers of amino acids, D-isomers are considered to behave as unnatural amino acids, like the amino acid analogs mentioned above. In previous reports in the 1980s, in vivo and in vitro experiments using ^{14}C-labeled D-amino acids revealed that the accumulation of D-isomers was higher than that of L-isomers in tumor cells [15,16]. At that time, the potential of D-isomers of amino acids as nuclear imaging agents was mentioned [15–17]. However, the precise mechanism responsible for the higher accumulation of the D-isomers has remained unclear. Recently, the biological functions of D-isomers in the central nervous system [18], developmental biology [19] and some pathological conditions [20,21] were reported, although the precise behavior of D-isomers still remains to be clarified [22].

Amino acid transport across the plasma membrane is mediated via amino acid transporters located on the membrane. Among the amino acid transport systems, system L, a Na^+-independent neutral amino acid transporter system, is the major route for providing cells with large neutral amino acids including branched or aromatic amino acids [23]. Recently, system L amino acid transporters 1 and 2 (LAT1 and LAT2) were isolated, and their characteristics were evaluated [24–26]. LAT1 was shown to be strongly expressed in malignant tumors [27,28] and also expressed in some normal organs such as brain, spleen, placenta and testis [29]. In contrast, the distribution of LAT2 mRNA is ubiquitous [30,31]. We previously reported that the D-isomer of *O*-[^{18}F]fluoromethyl-L-tyrosine (D-[^{18}F]FMT) was highly accumulated in tumor tissue [32,33], although the accumulation of D-[^{18}F]FMT in normal tissues, e.g., brain, kidney and pancreas, was low as was the whole-body background. However, the molecular mechanism of D-[^{18}F]FMT uptake in tumor tissue was not addressed at that time. Since the presence of amino acids in plasma would affect the uptake of this tracer into tissues, the concentrations of amino acids in plasma, in normal and tumor tissues, and in the microenvironment of tumor cells must be considered [34].

In this study, the characteristics and utility of the D-isomer of an artificial amino acid labeled with ^{18}F positron emitter were evaluated; and the behavior of L-[^{18}F]FMT and D-[^{18}F]FMT both in vitro and in vivo was examined.

2. Materials and methods

2.1. Materials

L-Alanine, L-glycine, L-phenylalanine, L-serine, D-leucine and L-leucine were purchased from Wako Pure Chemical Co. Ltd. (Osaka, Japan). 2-Aminobicyclo-(2,2,1)-heptane-2-carboxylic acid (BCH) was obtained from Sigma-Aldrich Japan (Tokyo, Japan). All other reagents were of analytical grade.

2.2. Synthesis of labeled compound

Positron-emitting ^{18}F was produced by $^{18}O(p,n)^{18}F$ nuclear reaction using the cyclotron (HM-18; Sumitomo Heavy Industry, Japan) at Hamamatsu Photonics PET Center. L- and D-Isomers of [^{18}F]FMT were synthesized by reacting [^{18}F]fluoro-methyl bromide with the corresponding L- and D-tyrosine according to a previous report [32,33]. Enantiomeric purity was analyzed on a CHIOBIOTIC T column (4.6×250 mm; Tokyo Kasei Kogyo). The elution solution was ethanol/water (1:1), and the flow rate was 1 ml/min. The production of [^{18}F]FDG was performed according to the method reported previously [35]. Specific activities of D-[^{18}F]FMT, L-[^{18}F]FMT and [^{18}F]FDG were 115±10, 126±12 and 144±21 GBq/μmol, respectively; and radiochemical purities were 99.6±0.4%, 99.8±0.3% and 100.0±0.0%, respectively.

2.3. Cell culture

C6 glioma cells (ATCC, Rockville, MD, USA) and HeLa cells (RIKEN, Tsukuba, Japan) were grown in Dulbecco's Modified Eagle's Medium (DMEM, Wako) supplemented with 10% fetal bovine serum (Japan Bioserum, Hiroshima, Japan) and appropriate concentrations of antibiotics (100 U/ml penicillin and 100 μg/ml streptomycin). The cells were maintained in plastic culture flasks at 37°C in a humidified atmosphere containing 5% CO_2 and kept as monolayers.

2.4. Measurement of uptake by cells in culture

Rat C6 glioma cells and HeLa cells were plated in 24-well culture plates (Corning Japan, Tokyo, Japan) at a density of 2×10^5 cells per well and cultured for 24 h. After the growth medium had been removed, the cells were washed twice with Hank's balanced salt solution (HBSS; 136.6 mM NaCl, 5.4 mM KCl, 4.2 mM $NaHCO_3$, 1 mM $CaCl_2$, 0.5 mM $MgCl_2$, 0.44 mM KH_2PO_4 and 0.41 mM $MgSO_4$) and kept in HBSS for 30 min at 37°C to deplete any residual nutrients from the growth medium. Then the HBSS was discarded, and the uptake assay was started by adding a trace amount of D- or L-isomer of [^{18}F]FMT/HBSS (1–3 MBq/ml) to the cultures. After incubation for the selected time period (2, 5, 10, 30 and 60 min), the uptake of labeled compounds was terminated by removing the medium. After the cells had been washed twice with 1 ml of ice-chilled Dulbecco's phosphate-buffered saline (PBS), the cells were lysed in 400 μl of cell lysis solution (0.1 M NaOH, 2% Triton X-100). The radioactivity in the cell lysates was measured by a γ-counter (Aloka ARC-2000). More than three independent experiments, each done in triplicate, were performed.

2.5. Tracer release from cultured cells

Experiments were performed using 24-well culture plates. HeLa cells (2×10^5 cells/well) were incubated with D- or L-isomer of [^{18}F]FMT (1-3 MBq/ml) in HBSS for 30 min at 37°C. Then, the cells were washed three times with HBSS, and all supernatants were discarded. Release experiments were started by the addition of 1 ml HBSS. The supernatant

was collected at each time point from each well, and cells in the well were washed twice with ice-chilled PBS very quickly. Then the cells were lysed with 400 μl of cell lysis solution (0.1 M NaOH, 2% Triton X-100), and the radioactivity in the cell lysates was measured by a γ-counter. More than three independent experiments, each done in triplicate, were performed.

2.6. Reverse transcriptase–polymerase chain reaction

Total RNAs were isolated from C6 glioma and HeLa cells by using an RNA purification kit (QIAshredder and RNeasy kit, QIAGEN KK, Tokyo, JAPAN) in accordance with the manufacturer's instructions. Then, the first-strand cDNAs were prepared with a Superscript First-strand Synthesis system (Invitrogen Japan KK, Tokyo, Japan) and oligo(dT) primer, and used as a template for polymerase chain reaction (PCR) amplification. The PCR amplification was performed with Ex Taq (Takara Bio, Inc., Ohtu, Japan) according to the following protocol [27]: 94°C for 5 min, followed by 25 cycles of 94°C for 30 s, 60°C for 30 s and 72°C for 1 min and a final extension step of 72°C for 10 min. The following primer pairs were used for PCR amplification: 5′-CAATGGTGTGGCCATCATG-3′ and 5′-GATGCATCCCCTTGTCCTAT-3′ for rat LAT1, 5′-TCATTGGCTCCGGAATCTTC-3′ and 5′-ATGCA TTCTTTGGCTCCAGC-3′ for rat LAT2, 5′-TCACAGGCT-TATCCAAGGAG-3′ and 5′-TACAATGTCAGCCTGAG-GAG-3′ for rat 4F2hc, 5′-TTCATCGCA- GTACATCG-TGG-3′ and 5′-CCCAGGTGATAGTTCCCGAA-3′ for human LAT1, 5′-AGCCCTGAAGAAAGAGATCG-3′ and 5′-TGCATATCTGTACAATCCCC-3′ for human LAT2, 5′-TCGATTACCTGAGCTCTCTG-3′ and 5′-GGGATTTTG-TATGCTCCCCA-3′ for human 4F2hc and 5′-TGACGGGGTCACCCACACTGTGCCCATCTA-3′ and 5′-CTAGAAGCATTTGCGGTGGACGATGGAGGG-3′ for human and rat β-actin.

2.7. Animals

All animals were maintained and handled in accordance with the recommendations of the National Institutes of Health and the Animal Facility Guidelines of the University of Shizuoka.

The mice bearing tumors were prepared as reported previously [32]. Briefly, female BALB/cA Jcl-nu mice (7 weeks old) were inoculated subcutaneously with 5×10^6 HeLa cells, maintained for 2 weeks after the transplantation and used for experiments at 9 weeks of age.

Male Fischer rats (9 weeks old) were obtained from Japan SLC, Inc. The rat C6 brain tumor model was prepared as reported elsewhere with a minor modification [36]. Rats were anesthetized with chloral hydrate and individually placed in a stereotaxic apparatus. C6 glioma cells (2×10^5 cells/10 μl of DMEM containing 1% gelatin) were injected at a rate of 1.0 μl/min into the left hippocampus of the rat (−4.7 mm posterior to bregma, −3.9 mm lateral to the midline suture and −6.2 mm from the dura) via a 28-gauge stainless tube. Eleven days after tumor implantation, the rats were used for PET studies.

2.8. Whole-body imaging of tumor-bearing mice and rats

The distribution pattern of each radiolabeled compound in the rats was determined with a small-animal PET system (Clairvivo PET, Shimadzu, Kyoto, Japan). Animals were anesthetized by an intraperitoneal injection of chloral hydrate at 400 mg/kg, followed by continuous infusion of the anesthetic at 100 mg/kg per hour through a cannula placed into a tail vein. Anesthetized rats were fixed on an animal holder. Each ^{18}F-radiolabeled compound at a dose of 7 MBq was injected intravenously into each rat via a tail vein. The data were obtained with a list mode data acquisition every 1 s for 60 min. Reconstruction was made by 3D-DRAMA (two iterations, γ=0.1) with resolution modeling. After the PET analysis, the rat brains were excised and sliced into eight coronal slices of 2-mm thickness (four slices anterior to and four slices posterior to the optical chiasm) with a brain slicer (Muromachi Kikai, Co. Ltd, Tokyo, Japan). The distribution of [^{18}F]FMT or [^{18}F]FDG in each brain slice was determined by autoradiography after exposure to an imaging plate for approximately 1 h. The autoradiograms of the brain slices were obtained by using a Bio-imaging analyzer BAS1500 and analyzed by Image Gauge V3.45 (Fuji Photo Film, Co. Ltd, Tokyo, Japan).

3. Results

3.1. Uptake and release of [^{18}F]FMT in vitro

The enantiomeric purity of each isomer was determined by the enantiomeric analytic HPLC as reported previously [33]. The results showed the enantiomeric purity of each isomer to be more than 98%.

At first, we examined the transport of the D- and L-isomers of [^{18}F]FMT in rat C6 glioma cells and HeLa cells. The uptake of D- and L-isomers of [^{18}F]FMT into these cells was measured at selected time points up to 30 min. As a result, the uptake rate of the L-isomer was significantly higher than that of the D-isomer in both C6 glioma and HeLa cells (Fig. 1). The uptake was not saturated at least up to 60 min (data not shown).

Then, the release of the D- and L-isomers from HeLa cells in the presence or absence of 100 μM L-leucine was examined. As shown in Fig. 2A, the release of the D-isomer under the amino acid-free condition in HBSS was slower than that of L-isomer. On the other hand, the release rate of both L-[^{18}F]FMT and D-[^{18}F]FMT was accelerated in the presence of L-leucine (Fig. 2B). These uptake and release experimental results on [^{18}F]FMT indicate that the amino acid transport activity of the D-isomer was lower than that of the L-isomer in both C6 glioma and HeLa cells in vitro. Then, we further examined the selectivity of the transporter by performing inhibition experiments in C6 glioma cells. The uptake of D- and L-isomers of [^{18}F]FMT was strongly inhibited in the presence of 1 mM L-isomers of methionine, phenylalanine and tyrosine (Fig. 3A). The uptake was also

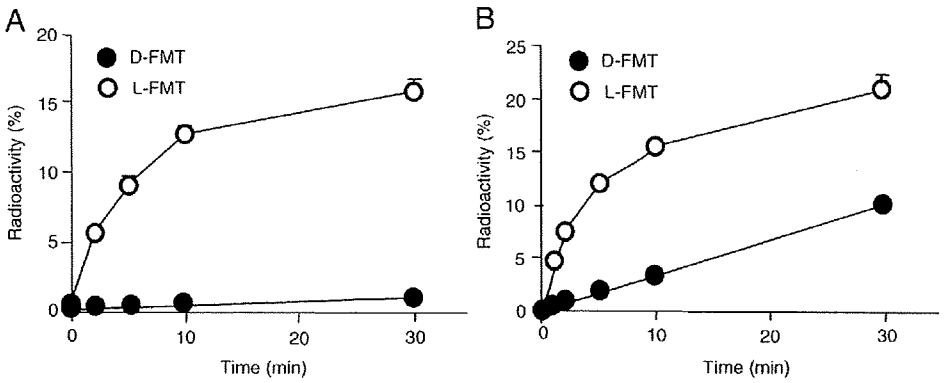

Fig. 1. Time-dependent uptake of D- and L-isomers of [^{18}F]FMT by C6 glioma and HeLa cells. The C6 glioma (A) and HeLa (B) cells were incubated for 1, 2, 5, 10 or 30 min in uptake solution containing 1–3 MBq of D- or L-isomers of [^{18}F]FMT. The relative radioactivity (as a percentage of the total dose) at each point is indicated as the mean±S.D. More than three independent experiments, each done in triplicate, were performed.

inhibited by BCH, a selective inhibitor of the system L amino acid transporter. However, the uptake was not inhibited by L-glycine. These inhibition patterns in the presence of amino acids for uptake of D- and L-isomers of [^{18}F]FMT were essentially the same, suggesting that both D- and L-isomers of [^{18}F]FMT were taken up by the same transporter, namely, the system L amino acid transporter.

Since the activity of the system L amino acid transporter is reported to be independent of extracellular sodium ions [24,25], we next examined the sodium ion dependency of the D- and L-[^{18}F]FMT transport. A sodium ion-free condition was obtained by substitution of sodium chloride with choline chloride, as reported previously [25]. Fig. 3B shows the sodium ion-independent uptake of both D- and L-isomers. These results support the idea that both D- and L- isomers of [^{18}F]FMT are transported by system L amino acid transporters.

Next, the effect of the competitive inhibition of the system L amino acid transporter on the uptake of D- or L-isomer of [^{18}F]FMT was examined. D-[^{18}F]FMT or L-[^{18}F]FMT was loaded into HeLa cells in the presence of the various concentrations of BCH, a selective inhibitor of system L (Fig. 4A). The uptake of both D- and L-isomers of [^{18}F]FMT was inhibited by BCH in a dose- dependent manner. Furthermore, the inhibitory effect of various concentrations of natural amino acids, i.e., D- and L-leucine, on isomer uptake was examined. Both D- and L-leucine inhibited the uptake of [^{18}F]FMT; however, L-[^{18}F]FMT uptake was decreased more at a low concentration of the extracellular amino acids (Fig. 4B and C) than the D-isomer. These results suggest that the transport of L-[^{18}F]FMT was more affected in the presence of either L-leucine or D-leucine than that of the D-isomer in vitro and that this might also be the case in vivo.

System L amino acid transporter proteins LAT1 and LAT2 were isolated previously. LAT1 and LAT2 require an additional single-membrane-spanning protein heavy chain of the 4F2 antigen (4F2hc) for their functional expression in the plasma membrane. LAT1 and 4F2hc or LAT2 and 4F2hc form a heterodimeric complex via a disulfide bond. So we examined the mRNA expression of the system L amino acid transporters in C6 glioma and HeLa cells. In the reverse

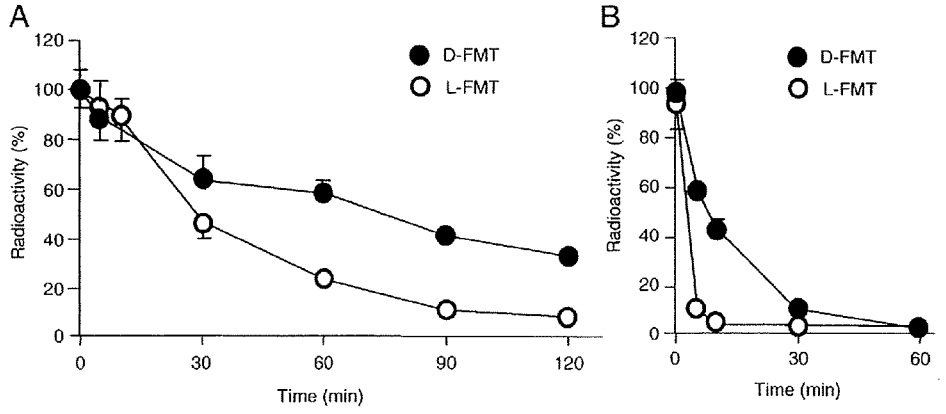

Fig. 2. Release of D- and L-isomers of [^{18}F]FMT preloaded in HeLa cells. The release of preloaded [^{18}F]FMT from HeLa cells was examined. The cells preloaded with D- or L-isomers of [^{18}F]FMT were incubated in the absence (A) or presence (B) of 100 μM L-leucine. The relative radioactivities that remained in the cells were determined to obtain the release rate of [^{18}F]FMT. Each point indicates the mean±S.D. More than three independent experiments, each carried out in triplicate, were performed.

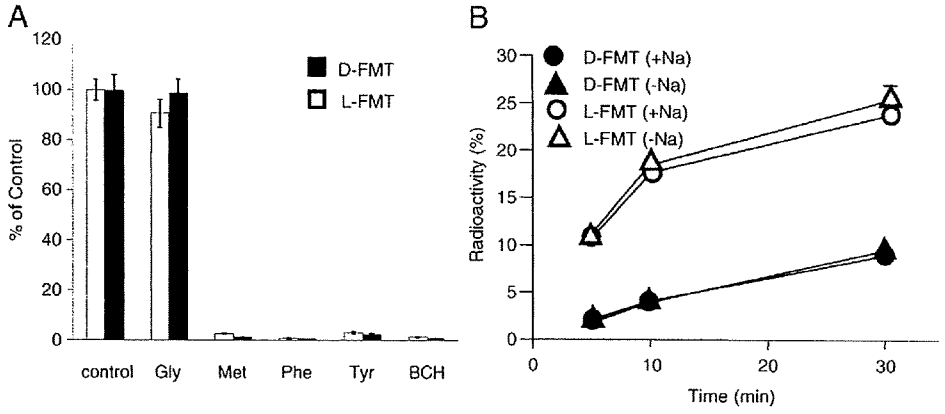

Fig. 3. Uptake of D- and L-isomers of [^{18}F]FMT by C6 glioma cells in the presence of amino acids, inhibitors and Na^+ ions. (A) C6 glioma cells were incubated with D- or L-isomer of [^{18}F]FMT in the uptake solution containing L-glycine, L-methionine, L-phenylalanine, L-tyrosine or BCH (100 μM for each). The relative radioactivity in the cells was determined. (B) C6 glioma cells were incubated with D- or L-isomer of [^{18}F]FMT in the uptake solution in the presence (circles) or absence (triangles) of Na^+ ions. The relative radioactivity of cells was determined. Data are presented as the relative mean uptake±S.D.

transcriptase–PCR (RT-PCR) analysis, the PCR products for LAT1 and their associating protein 4F2hc, but not the LAT2 product, were detected when RNA from the rat C6 glioma and HeLa cell cultures was used (Fig. 5).

3.2. Tumor PET imaging with [^{18}F]FMT

Noninvasive real-time imaging with a small-animal PET provides distribution data consistent with those obtained from tissue dissection assays. Mice xenografted with HeLa cells were prepared and examined by PET. Data were acquired from mice administered D-[^{18}F]FMT, L-[^{18}F]FMT or [^{18}F]FDG (Fig. 6). The mouse injected with D-[^{18}F]FMT showed the clearest difference in tracer intensity between the tumor (right leg) and the normal tissue (left leg) compared with the mice given the other tracers. The accumulation of D-[^{18}F]FMT in the tumor tissue was not different from that of L-[^{18}F]FMT. The standard uptake value (SUV) of the former was 1.336; and that of the latter, 1.642. However,

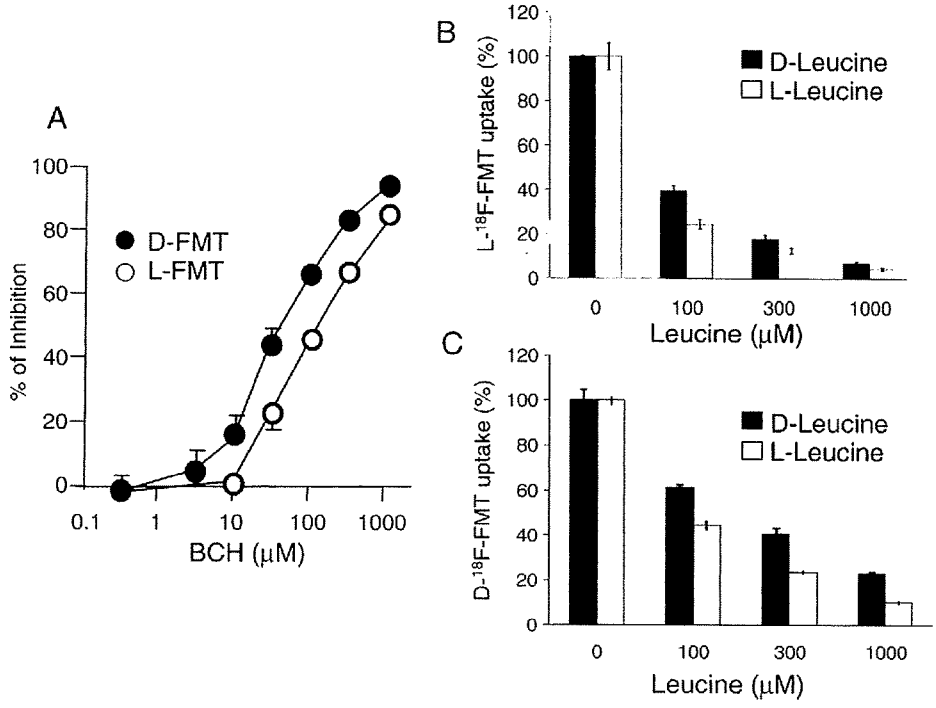

Fig. 4. BCH- and L- or D-leucine-mediated inhibition of D- or L-[^{18}F]FMT uptake by HeLa cells. The uptake of D- (open circle) or L-isomer (closed circle) of [^{18}F]FMT was measured for 5 min in the presence of various concentrations of BCH (A). The stereo-selective inhibitory effect of leucine on the uptake of L-[^{18}F]FMT (B) and D-[^{18}F]FMT (C) into HeLa cells was examined in the presence of 0, 100, 300 and 1000 μM L- or D-leucine. The graph shows the % radioactivity of the control (without leucine). Bars indicate the mean±S.D.

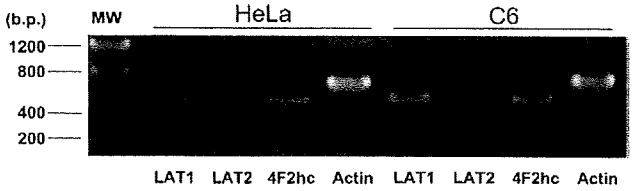

Fig. 5. RT-PCR detection of LAT1, LAT2 and 4F2hc mRNAs in HeLa and C6 cells. First-strand cDNAs prepared from cultured C6 glioma and HeLa cells were used as templates for PCR amplification. The PCR products were subjected to agarose gel electrophoresis and visualized with ethidium bromide.

there was far less radioactivity in the normal tissue in the case of the image obtained with the D-isomer of [^{18}F]FMT: SUVs for D-[^{18}F]FMT and L-[^{18}F]FMT were 0.488 and 0.874, respectively.

Finally, the in vivo tumor imaging in the brain tumor model was examined. Data were displayed as the image of

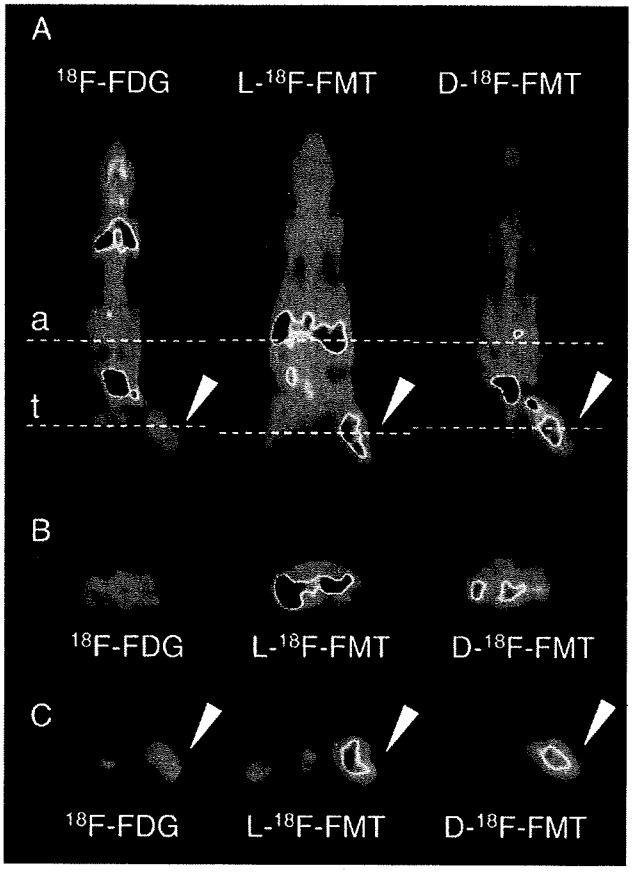

Fig. 6. Small-animal PET images of [^{18}F]FDG, L-[^{18}F]FMT and D-[^{18}F]FMT in tumor-bearing mice. Mice were inoculated with HeLa cells, and radiolabeled compounds were injected intravenously for the PET imaging. Coronal plane images (A), axial plane images of the abdominal region (B) and axial plane images of tumor implanted region (C) after injection of [^{18}F] FDG, L-[^{18}F]FMT or D-[^{18}F]FMT are shown. The broken lines "a" and "t" indicate the position of the axial plane image of the abdominal region (B) and the tumor region (C), respectively. The arrowhead points to the tumor. The typical images from multiple independent experiments (n>3) are shown.

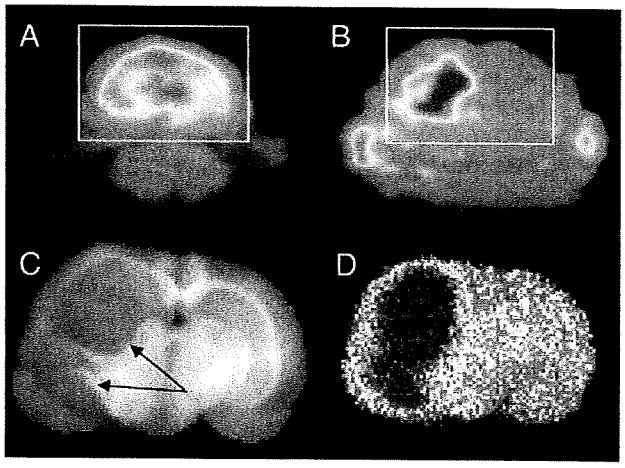

Fig. 7. Small-animal PET images of D-[^{18}F]FMT and [^{18}F]FDG in a brain tumor-bearing rat. PET imaging of [^{18}F]FDG (A) and D-[^{18}F]FMT (B) was performed in the same rat bearing a C6 glioma brain tumor. The brain area in the PET image is indicated by the square. After the PET study with D-[^{18}F] FMT, brain slices were prepared to confirm the location of the tumor (arrows, C) and to detect the radioactivity of D-[^{18}F]FMT in the brain by autoradiography (D). Note that images in (C) and (D) are expanded beyond the square region (brain). Five separate experiments were performed, and similar results were obtained. Data typical of one of them are shown here.

the D-isomer of [^{18}F]FMT in comparison with that of [^{18}F] FDG in the rat C6 glioma orthotopic brain tumor model, as shown in Fig. 7. In this model of brain tumor, [^{18}F]FDG could not detect the tumor specifically due to the high background in the normal brain tissue (Fig. 7A). In contrast, D-[^{18}F]FMT showed a lower accumulation in the normal region of the brain (Fig. 7B), and thus the tumor region in the brain was imaged. (Comment in Fig. 7C and D).

4. Discussion

In the present study, we investigated the properties of ^{18}F-labeled D- and L-isomers of artificial amino acid FMT in relation to their transport activity in cultured C6 glioma and HeLa cells. In addition, the specificity of amino acid transporters engaged in the transport of D- and L-isomers of [^{18}F]FMT was examined.

Concerning ^{18}F-PET studies, positron emitter-labeled diagnostic drugs possess very high specific radioactivity: specific activities of D-[^{18}F]FMT, L-[^{18}F]FMT and [^{18}F]FDG in the present study were 115±10, 126±12 and 144±21 GBq/μmol, respectively. Therefore, the experiment was performed by using amino acids at the tracer level concentration. The uptake study on the D- and L- isomers of [^{18}F]FMT in C6 glioma and HeLa cells in HBSS suggested that the incorporation was mediated by a stereo-selective amino acid transporter, since the L-isomer was incorporated much faster than the D-isomer (Fig. 1).

The release of D- and L-isomers of [^{18}F]FMT was examined by use of HeLa cells preloaded with each isomer